Accelerator, reactor, solar, and atmospheric neutrino oscillations: Beyond three generations

Srubabati Goswami
Department of Pure Physics, University of Calcutta, 92 Acharya Prafulla Chandra Road, Calcutta 700 009, India
(Received 20 August 1996)

We perform a phenomenological analysis of neutrino oscillations introducing an additional sterile neutrino. In such a scenario, more than one spectrum is possible that can accommodate three hierarchically different mass-squared differences as required by the present experiments. We considered two different spectra. Choosing the $\Delta m^2 s$ in the ranges suitable for the LSND, atmospheric, and solar neutrino oscillations, limits on the mixing angles are derived, consistent with the most restrictive accelerator and reactor data as well as the atmospheric and solar neutrino results. We show that the present data disfavor one of these mass spectra leaving us with a very stringent choice of mass and mixing angle. The potential of the future heavy water solar neutrino experiment SNO to distinguish between the four-neutrino mixing and two-neutrino mixing cases is explored. [S0556-2821(97)01603-2]

PACS number(s): 14.60.Pq, 14.60.Lm, 26.65.+t, 96.40.Tv

I. INTRODUCTION

The question of whether or not neutrinos have a nonzero mass has remained one of the most tantalizing issues in present day physics. In the standard model of electroweak theory neutrinos are considered to be massless. But there is no compelling theoretical reason behind this assumption. Most extensions of the standard model allow a small but nonzero neutrino mass. A way for probing small neutrino masses and the mixing between different neutrino flavors is provided by neutrino oscillations. Considering only two generations for simplicity, the probability that an initial ν_α of energy E gets converted to a ν_β after traveling a distance L in vacuum is

$$P_{\nu_\alpha \nu_\beta} = \sin^2 2\theta \, \sin^2(1.27 \Delta m^2 L/E), \tag{1}$$

where θ is the mixing angle in vacuum. Δm^2 denotes the mass difference squared in eV^2. L/E is in meter/MeV. The oscillatory character is embedded in the second factor in Eq. (1). The detection of this phenomenon in an experiment requires $E/L \simeq \Delta m^2$.

Recently the Liquid Scintillator Neutrino Detector (LSND) Collaboration has declared its results for a positive evidence of $\overline{\nu_\mu}$-$\overline{\nu_e}$ oscillations [1] (see, however, [2]). Prior to this, indications of neutrino oscillations came from the well-known solar neutrino problem and the atmospheric neutrino anomaly.

If indeed neutrino flavor oscillations take place, the most sensitive value of Δm^2 for detecting such a phenomenon in LSND is in the eV^2 range, which is in the right area for the cold plus hot dark matter scenario for structure formation in the early universe [3]. It remains to be seen whether the LSND results stand the test of time [4] but already this has added a new impetus to the issue of neutrino mass and mixing and a number of investigations have been carried out recently, discussing the possible impact of this on particle physics, astrophysics, and cosmology [5].

The observed suppression of solar neutrino fluxes as compared to the theoretical predictions constitutes the long-standing solar neutrino problem. A purely astrophysical solution to this, attributing the deficit to an inaccurate prediction of the fluxes by the standard solar models [6,7], is disfavored by the present data [8]. If neutrinos are massive, a plausible explanation to the solar neutrino problem is neutrino oscillations in vacuum [9] or the Mikheyev-Smirnov-Wolfenstein (MSW) [10] effect of matter enhanced resonant flavor conversions. The basic idea is the transition of ν_e to another species—active or sterile—to which the detector is not sensitive. The two-generation oscillation explanation for the solar neutrino problem requires $\Delta m^2 \sim 5.4 \times 10^{-6}$ eV^2 and $\sin^2 2\theta \sim 7.9 \times 10^{-3}$ (nonadiabatic solution) and $\Delta m^2 \sim 1.7 \times 10^{-5}$ eV^2 and $\sin^2 2\theta \sim 0.69$ (large-mixing-angle solution) [11] for the MSW transition to an active neutrino. If instead one considers oscillations to sterile neutrinos as a possible solution, the large-angle region is excluded at 98–99 % C.L. [12]. Oscillations in vacuum to an active neutrino require $\Delta m^2 \sim 0.615 \times 10^{-10}$ eV^2 and $\sin^2 2\theta \sim 0.864$ [13]. The sterile neutrino alternative for this case is ruled out by the present data at 95–98 % C.L [13,14].

The primary components of the cosmic-ray flux interact with the Earth's atmosphere, producing pions and kaons which can decay as

$$\pi^\pm (K^\pm) \to \mu^\pm + \nu_\mu (\overline{\nu_\mu}), \quad \mu^\pm \to e^\pm + \nu_e (\overline{\nu_e}) + \overline{\nu_\mu} (\nu_\mu).$$

These neutrinos can be detected by imaging water Čerenkov detectors—Kamiokande [15,16] and IMB [17]—or using iron calorimeters as is done in Fréjus [18], Nusex [19], and Soudan2 [20]. To reduce the uncertainty in the absolute flux values the usual practice is to present the ratio of ratios R [21]:

$$R = \frac{(\nu_\mu + \overline{\nu_\mu})/(\nu_e + \overline{\nu_e})_{\mathrm{obsvd}}}{(\nu_\mu + \overline{\nu_\mu})/(\nu_e + \overline{\nu_e})_{\mathrm{MC}}}, \tag{2}$$

where MC denotes the Monte Carlo–simulated ratio. Kamiokande and IMB find R to be less than the expected value of unity. This deviation is known as the atmospheric neutrino anomaly. Preliminary results from Soudan2 agree with this but Fréjus and Nusex results are consistent with theoretical predictions. The atmospheric anomaly, if it exists, can be

explained by either ν_μ-ν_e or ν_μ-ν_τ oscillations in a two-generation picture. The analysis of the new multi-GeV data as well as the previous sub-GeV data of the Kamiokande Collaboration predicts the best-fit parameters $(\Delta m^2, \sin^2 2\theta) = (1.8\times10^{-2}\ \text{eV}^2, 1.0)$ for ν_μ-ν_e oscillations and $(1.6\times10^{-2}\ \text{eV}^2, 1.0)$ for ν_μ-ν_τ oscillations [16]. Since the required mixing angle is large, oscillations to sterile neutrinos for this case as well as for the large-angle MSW and vacuum oscillation solutions were believed to be inconsistent with the nucleosynthesis constraints [22]. However, this conclusion depends on the bound on the number of neutrino species from big bang nucleosynthesis [23,24]. If N_ν is <4, then mixing with a sterile species is required to be suppressed strongly. If, on the other hand, $N_\nu > 4$ as suggested recently in [25], the possibility of large mixing with sterile neutrinos cannot be excluded *a priori* (see also [26]).

The three neutrino oscillation phenomena mentioned above—namely, the solar neutrino problem, the atmospheric neutrino anomaly, and the $\overline{\nu_\mu}$-$\overline{\nu_e}$ oscillations observed by the LSND group—require three hierarchically different mass ranges which cannot be accommodated in a three-generation picture and many of the studies after the declaration of the LSND results attempted a simultaneous explanation of any two of the above—the solar plus accelerator and reactor data [27] or atmospheric plus accelerator and reactor data [28,29]. A recent combined three-generation analysis of solar and atmospheric neutrino oscillation data can be found in [30–33]. Another approach is to use one common mass scale to explain the accelerator and reactor as well as atmospheric neutrino oscillations. The other independent mass scale is employed to explain the solar neutrino oscillations [33–37]. As discussed in [37] the common mass-squared difference needed for a simultaneous explanation of the accelerator, reactor, and atmospheric neutrino data lies in the range ~ 0.2–$0.4\ \text{eV}^2$, which is one order of magnitude lower than the value most commonly associated with LSND and one order of magnitude larger than the mass scale of $10^{-2}\ \text{eV}^2$ known to be the best-fit value from two-generation studies of atmospheric neutrino oscillations [16]. A recent three-generation analysis of the sub-GeV as well as multi-GeV Kamiokande data including matter effects also indicates a best-fit Δm^2 of $10^{-2}\ \text{eV}^2$ [38]. It has been widely realized that a remedy of this situation might be the introduction of a fourth neutrino. LEP data reveal that there are three light active neutrino species. So the fourth neutrino has to be sterile.

Introducing this additional neutrino one can attempt to separate two-generation treatments for each but a more comprehensive approach would be to determine the parameter ranges consistent with all the experiments by a combined analysis in a four-neutrino framework, which can reveal the full implications of each experimental datum on the others. In this paper we perform such an oscillation analysis. Phenomenological analyses involving four massive neutrinos have been carried out earlier in Ref. [39] and more recently in Refs. [40,41].

In a scenario with four neutrinos there are six Δm^2's, three of which are independent, and six mixing angles, neglecting CP-violating phases. We assume a minimal four-neutrino mixing scheme, in which the sterile neutrino mixes only with the electron neutrino, thus reducing the number of mixing angles to 4. We do not make any assumptions regarding these mixing angles, allowing them to cover the whole range from 0 to $\pi/2$. Guided by the present data on neutrino oscillation we consider two different sets of hierarchical mass squared differences.

(i) Mass pattern. $\Delta_{13} \simeq \Delta_{23} \simeq \Delta_{34} = \Delta_L$, the largest mass scale, in the LSND range, $\Delta_{12} \simeq \Delta_{24} = \Delta_I$, the intermediate mass scale as preferred by the atmospheric neutrino data, and $\Delta_{14} = \Delta_S$, the smallest mass scale, either in the MSW or in the vacuum oscillation range.

(ii) Mass pattern. $\Delta_{12} \simeq \Delta_{13} \simeq \Delta_{24} \simeq \Delta_{34} = \Delta_L$, $\Delta_{23} = \Delta_I$, $\Delta_{14} = \Delta_S$. $\Delta_{ij} = |m_j{}^2 - m_i{}^2|$. The hierarchy in the absolute values of neutrino masses as implied by the above spectra can be classified in general as follows.

Case (i): (a) $m_4^2 \simeq m_1^2 \approx m_2^2 \ll m_3^2$ or (b) $m_4^2 \simeq m_1^2 \approx m_2^2 \gg m_3^2$.

Case (ii): (a) $m_4^2 \simeq m_1^2 \ll m_2^2 \approx m_3^2$ or (b) $m_4^2 \simeq m_1^2 \gg m_2^2 \approx m_3^2$.

These are shown schematically in Fig. 1. The $\simeq$ and $\approx$ signs imply that differences by Δ_S and Δ_I are neglected, respectively, while the $\gg$ or $\ll$ sign means difference by Δ_L. In each case, the scenarios (a) and (b) differ only in that the signs of all Δ_{ij}'s are opposite. Neutrino oscillation analysis remains the same for (a) and (b) in both cases and one has to invoke some other experimental constraints like that from neutrinoless double β decay for a distinction between these [28].

Models for neutrino masses and mixings assuming the existence of sterile states besides the three active flavors have been discussed before [42]. After the declaration of the LSND results models involving extra singlet neutrinos have been constructed by many authors [43]. Our investigation is not motivated by any particular model. Rather, we do a phenomenological analysis in which we fix the two Δm^2's related to the atmospheric and LSND signals at appropriate representative values and determine the other oscillation parameters from the experimental data. We would like to emphasize that the two mass differences related to atmospheric and LSND signals have not been fitted but simply fixed to representative values in the analysis (while all the other oscillation parameters have been fitted).

The plan of the paper is as follows. In Sec. II we summarize the experimental results relevant for our purpose. In the following section we calculate the survival and transition probabilities for the various experiments for the mass spectra (i) and (ii). The results of our analysis and some discussions are presented in Sec. IV where we also examine whether the future solar neutrino experiment SNO can differentiate between the two-neutrino and four-neutrino models. We end in Sec. V with a short summary and conclusions.

II. EXPERIMENTAL RESULTS

A. Laboratory experiments

The laboratory experiments can serve as an important tool for neutrino oscillation search. These are either accelerator or reactor based and in general are of two types: (i) disappearance experiments, in which one looks for a reduction in the initial neutrino flux due to oscillations to some other flavor to which the detector is not sensitive; (ii) appearance experi-

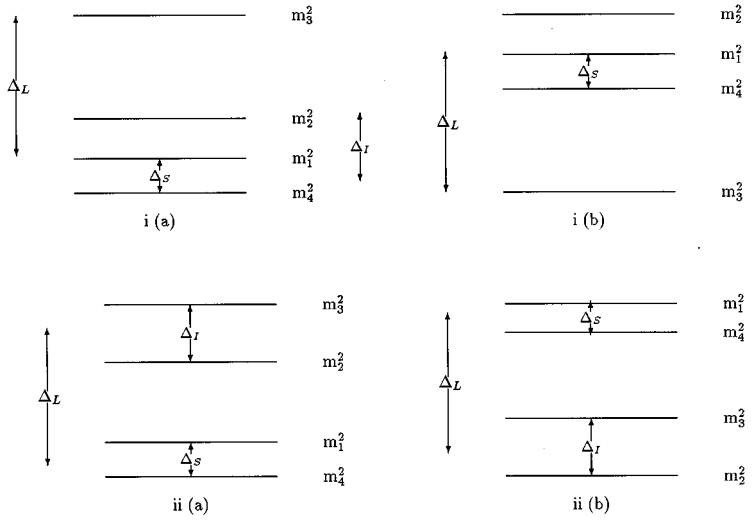

FIG. 1. The possible mass spectra considered (not to scale). The scenarios (a) and (b) are related as (a)$\leftrightarrow$(b) under $\Delta_{ij}\leftrightarrow-\Delta_{ij}$.

ments, in which one searches for a new neutrino flavor, absent in the initial beam, which can arise from oscillation.

Prior to the LSND results, all the laboratory experiments were consistent with no neutrino oscillations [44] and provided exclusion regions in the Δm^2-$\sin^2 2\theta$ plane. In the region of large Δm^2, the $\sin^2(1.27\Delta m^2 L/E)$ term $\rightarrow$ 0.5 and $P_{\nu_\alpha\nu_\beta}=0.5\sin^2 2\theta$. Thus the limits on $\sin^2 2\theta$ from the exclusion plots can be used to extract bounds on $P_{\nu_\alpha\nu_\beta}$. In Table I we summarize the laboratory experiments which give the most stringent bounds on $P_{\nu_\alpha\nu_\beta}$ in the mass ranges of interest. The Δm^2, to which these experiments are sensitive, depends on the L/E factor.

B. Atmospheric neutrinos

Among the experiments measuring the atmospheric neutrino flux, data of the most statistical significance have been collected by the Kamiokande and the IMB Collaborations. For neutrinos of energy less than $\sim$1 GeV, IMB finds $R=0.54\pm0.05\pm0.12$ [17] in agreement with the Kamiokande data $R=0.60^{+0.06}_{-0.05}\pm0.05$ in this energy range [15,16]. Recently the Kamiokande group has published the results of the measurement of the flux ratio in the multi-GeV energy range [16]. They found $R=0.57^{+0.08}_{-0.07}\pm0.07$, in good agreement with the sub-GeV value. Another aspect of this measurement that can independently point towards neutrino oscillation is the dependence of R on the zenith angle. The multi-GeV Kamiokande data reveal a dependence on the zenith angle unlike the sub-GeV data, though the statistical significance of this result has been questioned [45]. For the purpose of this paper we use the sub-GeV Kamiokande results for which matter effects are negligible for values of Δm^2's used in the analysis and the ''empty Earth approximation'' is applicable (see Sec. III B).

TABLE I. The characteristics of the most restrictive accelerator and reactor experiments.

Experiment	E	L
Bugey	$\sim$5 MeV	$\sim$40 m
CDHSW	$2<E<20$ GeV	$\sim$1 km
E776	1$-$10 GeV	$\sim$1 km
E531	$\sim$50 GeV	0.949 km
LSND	36–60 MeV	30 m

C. Solar neutrinos

At present there are four ongoing experiments that are measuring the flux of solar neutrinos. These experiments along with the measured rates and theoretical predictions from Ref. [7] are summarized in Table II. All the experiments indicate that the measured flux is less than the standard model predictions. The degree of depletion differs from experiment to experiment. Since each type of experiment is sensitive to different parts of the solar neutrino energy spectrum, it is plausible that the suppression mechanism is energy dependent.

III. SURVIVAL AND TRANSITION PROBABILITIES

For N neutrino generations expression (1) generalizes to

$$P_{\nu_\alpha\nu_\beta}=\delta_{\alpha\beta}-4\sum_{j>i}U_{\alpha i}U_{\beta i}U_{\alpha j}U_{\beta j}\sin^2\left(\frac{\pi L}{\lambda_{ij}}\right). \quad (3)$$

i,j vary from 1 to N for N generations:

$$\lambda_{ij}=2.47m(E_\nu/\mathrm{MeV})(\mathrm{eV}^2/\Delta_{ij}). \quad (4)$$

The actual form of the various survival and transition probabilities will depend on the spectrum of Δm^2 chosen and the explicit form of U. If Δm^2 is such that a particular $\lambda\gg L$, then the corresponding oscillatory term $\sin^2\pi L/\lambda\rightarrow0$, whereas $\lambda\ll L$ would imply a large number of oscillations and consequently the $\sin^2\pi L/\lambda$ term averages out to 1/2.

Neglecting CP-violating phases, U is real and, in the minimal mixing scheme, is a function of four angles and can be expressed in general as the product of four 4×4 rotation matrices R_{ij}. As a consequence of CPT and CP invariance there is no distinction between $P_{\nu_\alpha\nu_\beta}$, $P_{\overline{\nu_\alpha\nu_\beta}}$, $P_{\nu_\beta\nu_\alpha}$, and $P_{\overline{\nu_\beta\nu_\alpha}}$ in our analysis. The oscillations are characterized by

TABLE II. The solar neutrino data employed in the analysis and the theoretical predictions from Ref. [7].

	Homestake [SNU]	Kamioka [10^6 cm^{-2} s^{-1}]	GALLEX [SNU]	SAGE [SNU]
Observed rate	2.55 ± 0.25[a]	2.89 ± 0.42[b]	$77.1\pm8.5^{+4.4}_{-5.4}$[c]	69.0 ± 13[d]
BP95 SSM	9.3 ± 1.1	6.62 ± 1.06	137^{+7}_{-6}	137^{+7}_{-6}

[a]Ref. [46].
[b]Ref. [47].
[c]Ref. [48].
[d]Ref. [49].

three oscillation wavelengths λ_L, λ_I, and λ_S corresponding to the three mass scales Δ_L, Δ_I, and Δ_S in the problem. Since $\lambda \propto 1/\Delta m^2$ [see Eq. (4)], λ_L is the shortest wavelength corresponding to the largest mass scale Δ_L and similarly λ_S denotes the longest wavelength characterized by the smallest mass scale Δ_S. Before calculating the probabilities for each mass spectrum we note the following general points.

A. Accelerator and reactor neutrinos

For the accelerator and reactor neutrinos, the energy and length scales are such that λ_S and $\lambda_I \gg L$ and the oscillations driven by these mass scales are absent. Thus the one mass scale dominance often used in the context of accelerator and reactor neutrino oscillations [33,50] is a valid approximation, the oscillations being driven by λ_L. We further note that for Bugey $\lambda_L \ll L$ so that $\sin^2(\pi L/\lambda_L)$ averages to 1/2.

B. Atmospheric neutrinos

For the atmospheric neutrinos in the energy range ~ 0.1–1 GeV traveling through a distance in the range ~ 10–10^4 km, $\lambda_S \gg L$, and the oscillations driven by Δ_S are absent. Thus the probabilities in this case involve two mass scales Δ_L and Δ_I. In the context of the sub-GeV Kamiokande data the oscillatory terms are often replaced by their average value of 0.5 [51,31,28]. This is a good approximation for the $\sin^2 \pi L/\lambda_L$ term but not for the $\sin^2(\pi L/\lambda_I)$ term in our case at $\Delta_I = 10^{-2}$ eV^2. Thus an averaging over the incident neutrino energy spectrum, the zenith angle of the beam as well as the final lepton energy, is done following the procedure of [52]. The general expression of Eq. (2) for N flavors in terms of the neutrino transition and survival probabilities is

$$R = \frac{\langle P_{\nu_\mu \nu_\mu} \rangle + \dfrac{N^0_{e\mu}}{N^0_{\mu\mu}} \langle P_{\nu_\mu \nu_e} \rangle}{\langle P_{\nu_e \nu_e} \rangle + \dfrac{N^0_{e\mu}}{N^0_{ee}} \langle P_{\nu_\mu \nu_e} \rangle}, \tag{5}$$

where

$$\langle P_{\nu_\alpha \nu_\beta} \rangle = \frac{1}{N^0_{\alpha\beta}} \int \frac{d^2\phi_\alpha}{dE_\nu d\cos\theta_\nu} P_{\nu_\alpha \nu_\beta} \times \frac{d\sigma}{dE_\beta} \epsilon(E_\beta) dE_\nu dE_\beta d(\cos\theta_\nu) \tag{6}$$

and

$$N^0_{\alpha\beta} = \int \frac{d^2\phi_\alpha}{dE_\nu d\cos\theta_\nu} \frac{d\sigma}{dE_\beta} \epsilon(E_\beta) dE_\nu dE_\beta d(\cos\theta_\nu). \tag{7}$$

E_ν is the neutrino energy, and ϕ_α is the flux of atmospheric neutrinos ν_α. $\epsilon(E_\beta)$ is the detection efficiency of a final charged lepton state with energy E_β. σ is the interaction cross section for the reaction $\nu N \to l^\pm N'$. The sub-GeV fluxes of [53] and the charged current quasielastic cross sections from [54] are used. The detection efficiencies [15] are incorporated. In a general multigeneration analysis of atmospheric neutrinos matter effects might be important for the ν_μ-ν_e oscillation mode [55]. Assuming a matter density of 5 g/cm^3 and $E = 1$ GeV, the term relevant for matter effects, $2\sqrt{2} G_F n_e E \equiv 3.65 \times 10^{-4}$ eV^2. It has been shown in [56,57,36] that for contained atmospheric neutrino events matter effects are important for Δm^2 in the range $\sim 10^{-3}$–10^{-4} eV^2. Since both the Δm^2 relevant for us are outside this range, the empty-Earth approach is good enough for our purpose. A general three-generation analysis of atmospheric neutrinos including matter effects for both sub-GeV and multi-GeV Kamiokande data is performed in [38,58].

C. Solar neutrinos

1. Vacuum oscillations

For oscillation of solar neutrinos in vacuum λ_L and $\lambda_I \ll L$ and the terms involving these average out to 1/2.

2. MSW mechanism

Solving the neutrino propagation equations in matter for more than two generations and arbitrary values of neutrino masses is, in general, a nontrivial exercise. MSW analyses for three neutrino generations and the conditions under which it simplifies have been done by many authors [59,30]. A particularly simplifying assumption is one in which the problem reduces to an effective two-generation case [30,33]. In our model Δ_{14} is kept in the range suitable for solving the solar neutrino problem for both the mass spectra and Δ_{12}, $\Delta_{13} \gg \Delta_{14}$. Under these conditions MSW resonance occurs between the first and fourth states while the second and third states remain unaffected by matter. Thus ν_e-ν_s oscillation is the dominant mode for depletion of solar neutrinos. However, in a combined analysis, mixing of ν_e with ν_μ and ν_τ is also expected to affect the probabilities.

D. Mass Spectrum (i)

For this case we take

$$U=R_{23}R_{13}R_{12}R_{14}=\begin{pmatrix} c_{12}c_{13}c_{14} & s_{12}c_{13} & s_{13} & c_{13}c_{12}s_{14} \\ -c_{23}s_{12}c_{14}-s_{13}c_{12}s_{23}c_{14} & c_{12}c_{23}-s_{13}s_{12}s_{23} & s_{23}c_{13} & -c_{23}s_{12}s_{14}-s_{13}c_{12}s_{23}s_{14} \\ s_{12}s_{23}c_{14}-s_{13}c_{12}c_{23}c_{14} & -c_{12}s_{23}-s_{13}s_{12}c_{23} & c_{13}c_{23} & s_{12}s_{23}s_{14}-s_{13}c_{12}c_{23}s_{14} \\ -s_{14} & 0 & 0 & c_{14} \end{pmatrix}, \tag{8}$$

where $c_{ij}=\cos\theta_{ij}$ and $s_{ij}=\sin\theta_{ij}$, here and everywhere else in the paper. Let us now see what the probabilities for the various experiments are in this case.

1. Accelerator and reactor experiments

In this case,

$$P_{\bar{\nu}_e\bar{\nu}_e}=1-2s_{13}^2c_{13}^2 \quad \text{(Bugey)}, \tag{9}$$

$$P_{\bar{\nu}_\mu\bar{\nu}_\mu}=1-4s_{23}^2c_{13}^2(1-c_{13}^2s_{23}^2)\sin^2(\pi L/\lambda_L) \quad \text{(CDHSW)}, \tag{10}$$

$$P_{\bar{\nu}_\mu\bar{\nu}_e}=4c_{13}^2s_{13}^2s_{23}^2\sin^2(\pi L/\lambda_L) \quad \text{(LSND,E776)}, \tag{11}$$

$$P_{\bar{\nu}_\mu\bar{\nu}_\tau}=4c_{23}^2s_{23}^2c_{13}^4\sin^2(\pi L/\lambda_L) \quad \text{(E531)}. \tag{12}$$

2. Atmospheric neutrinos

In this case the relevant probabilities appearing in Eq. (5) are

$$P_{\nu_e\nu_e}=1-2c_{13}^2s_{13}^2-4c_{12}^2s_{12}^2c_{13}^4\sin^2(\pi L/\lambda_I), \tag{13}$$

$$P_{\nu_\mu\nu_e}=2c_{13}^2s_{13}^2s_{23}^2+4c_{13}^2c_{12}s_{12}(c_{23}c_{12}-s_{13}s_{12}s_{23}) \times(c_{23}s_{12}+s_{13}c_{12}s_{23})\sin^2(\pi L/\lambda_I), \tag{14}$$

$$P_{\nu_\mu\nu_\mu}=1-2c_{13}^2s_{23}^2+2c_{13}^4s_{23}^4-4(c_{23}c_{12}-s_{13}s_{12}s_{23})^2 \times(c_{23}s_{12}+s_{13}c_{12}s_{23})^2\sin^2(\pi L/\lambda_I). \tag{15}$$

3. Solar neutrinos

(a.) Vacuum oscillations. The electron neutrino survival probability in this case is

$$P_{\nu_e\nu_e}=c_{13}^4c_{12}^4P_{2\text{vac}}+s_{13}^4+s_{12}^4c_{13}^4, \tag{16}$$

where $P_{2\text{vac}}$ is of the form of the two-generation vacuum oscillation probability:

$$P_{2\text{vac}}=1-\sin^2 2\theta_{14}\sin^2(\pi L/\lambda_S). \tag{17}$$

(b.) MSW mechanism. If the mass hierarchies, mixing angles, and the density distributions are such that one has resonance between the first and fourth mass eigenstates, while the second and third mass eigenstates remain independent of matter density, then the mixing matrix in matter is $U_M=R_{23}R_{13}R_{12}R_{14M}$. The mixing between the first and fourth generations gets modified by the matter effects as

$$\tan 2\theta_{14m}=\frac{\Delta_{14}\sin 2\theta_{14}}{\Delta_{14}\cos 2\theta_{14}-2\sqrt{2}G_Fn_{\text{eff}}E}, \tag{18}$$

where we define n_{eff} as

$$n_{\text{eff}}=c_{13}^2c_{12}^2n_e-\tfrac{1}{2}n_n. \tag{19}$$

In the limit $c_{13},c_{12}\to 1$ this reduces to the two-generation expression [60]. From Eq. (18), the resonance condition between the first and fourth generations in the presence of the other two generations becomes

$$2\sqrt{2}G_Fn_{\text{eff}}E=\Delta_{14}\cos 2\theta_{14}. \tag{20}$$

The difference between this and the three-generation resonance is to be noted. While the three-generation resonance condition gets modified by one additional mixing angle here the mixing angles with the second as well as the third generation appear in the resonance condition through n_{eff}. The calculation of the survival probability $P_{\nu_e\nu_e}$ is then a straightforward generalization of the standard two- or three-generation MSW scenario and one gets

$$P_{\nu_e\nu_e}=c_{12}^4c_{13}^4P_{\text{MSW}}+s_{13}^4+s_{12}^4c_{13}^4, \tag{21}$$

$$P_{\text{MSW}}=0.5+[0.5-\theta(E-E_A)X]\cos 2\theta_{14}\cos 2\theta_{14M}. \tag{22}$$

$E_A=\Delta_{14}\cos 2\theta_{14}/2\sqrt{2}G_Fn_{\text{eff}}$ gives the minimum ν energy that can encounter a resonance inside the sun. X denotes the jump probability between the first and fourth mass eigenstates. For this we use the expression due to Petcov [61] which is suitable for an exponential density profile as in the Sun. This gives

$$X=\frac{\exp[-\pi\gamma_R(1-\cos 2\theta_{14})]-\exp[2\pi\gamma_R]}{1-\exp[-2\pi\gamma_R]}. \tag{23}$$

γ_R is given by

$$\gamma_R=\frac{\Delta_{14}}{2E}\frac{R_S}{(1/n_{\text{eff}})dn_{\text{eff}}/dz}, \tag{24}$$

where $z=r/R_S$, R_S being the solar radius. We note that unlike the case discussed in [30], the mixing angles c_{12}^2 and c_{13}^2 appear in the expression of the jump probability, via $n_{\rm eff}$ defined in Eq. (19).

E. Mass spectrum (ii)

In this case we take

$$U=R_{13}R_{12}R_{23}R_{14}=\begin{pmatrix} c_{12}c_{13}c_{14} & s_{12}c_{13}c_{23}-s_{13}s_{23} & c_{13}s_{12}s_{23}+s_{13}c_{23} & c_{13}c_{12}s_{14} \\ -s_{12}c_{14} & c_{12}c_{23} & c_{12}s_{23} & -s_{12}s_{14} \\ -s_{13}c_{12}c_{14} & -s_{13}s_{12}c_{23}-c_{13}s_{23} & -s_{12}s_{13}s_{23}+c_{13}c_{23} & -s_{13}c_{12}s_{14} \\ -s_{14} & 0 & 0 & c_{14} \end{pmatrix}. \tag{25}$$

We next calculate the probabilities for the various experiments.

1. Accelerator and reactor experiments

In this case,

$$P_{\bar{\nu}_e\bar{\nu}_e}=1-2c_{13}^2c_{12}^2+2c_{13}^4c_{12}^4 \quad \text{(Bugey)}, \tag{26}$$

$$P_{\bar{\nu}_\mu\bar{\nu}_\mu}=1-\sin^2 2\theta_{12}\sin^2(\pi L/\lambda_L) \quad \text{(CDHSW)}, \tag{27}$$

$$P_{\bar{\nu}_\mu\bar{\nu}_e}=4c_{12}^2s_{12}^2c_{13}^2\sin^2(\pi L/\lambda_L) \quad \text{(LSND,E776)}, \tag{28}$$

$$P_{\bar{\nu}_\mu\bar{\nu}_\tau}=4c_{12}^2s_{12}^2s_{13}^2\sin^2(\pi L/\lambda_L) \quad \text{(E531)}. \tag{29}$$

2. Atmospheric neutrinos

For the chosen mass spectrum and mixing the probabilities appearing in Eq. (5) are

$$P_{\nu_e\nu_e}=1-2c_{13}^2c_{12}^2+2c_{13}^4c_{12}^4-4(c_{13}s_{12}c_{23}-s_{13}s_{23})^2 \times(c_{13}s_{12}s_{23}+s_{13}c_{23})^2\sin^2(\pi L/\lambda_I), \tag{30}$$

$$P_{\nu_\mu\nu_e}=2c_{13}^2c_{12}^2s_{12}^2-4c_{12}^2c_{23}s_{23}(c_{13}s_{12}c_{23}-s_{13}s_{23}) \times(c_{13}s_{12}s_{23}+s_{13}c_{23})\sin^2(\pi L/\lambda_I), \tag{31}$$

$$P_{\nu_\mu\nu_\mu}=1-2c_{12}^2s_{12}^2-4c_{12}^4c_{23}^2s_{23}^2\sin^2(\pi L/\lambda_I). \tag{32}$$

3. Solar neutrinos

(a.) Vacuum oscillations. The electron neutrino survival probability in this case is

$$P_{\nu_e\nu_e}=c_{13}^4c_{12}^4P_{2\rm vac}+(s_{12}c_{13}c_{23}-s_{13}s_{23})^4 +(c_{13}s_{12}s_{23}+s_{13}c_{23})^4, \tag{33}$$

where $P_{2\rm vac}$ is given by Eq. (17).

(b.) MSW mechanism. In this case the mixing matrix in matter is $U_M=R_{13}R_{12}R_{23}R_{14M}$. For this case also the resonance can be assumed to happen between the first and fourth mass eigenstates whence the mixing angle θ_{14M} and the resonance condition continue to be given by Eqs. (18) and (20). The probability, however, is different and can be expressed as

$$P_{\nu_e\nu_e}=c_{12}^4c_{13}^4P_{\rm MSW}+(s_{12}c_{13}c_{23}-s_{13}s_{23})^4 +(c_{13}s_{12}s_{23}+s_{13}c_{23})^4, \tag{34}$$

where $P_{\rm MSW}$ is defined in Eq. (22).

TABLE III. The constraints on the angular factors of the most restrictive accelerator and reactor experiments at different values of Δ_L.

Experiment	LSND[a]	Bugey[b]	CDHSW[c]	E776[d]	E531[e]
Angle factor A [Mass spectrum (i)]	$4c_{13}^2s_{13}^2s_{23}^2$	$4s_{13}^2c_{13}^2$	$4s_{23}^2c_{13}^2(1-c_{13}^2s_{23}^2)$	$4c_{13}^2s_{13}^2s_{23}^2$	$4c_{23}^2s_{23}^2c_{13}^4$
Angle factor A [Mass spectrum (ii)]	$4c_{12}^2s_{12}^2c_{13}^2$	$4c_{12}^2c_{13}^2(1-c_{12}^2c_{13}^2)$	$4c_{12}^2s_{12}^2$	$4c_{12}^2s_{12}^2c_{13}^2$	$4c_{12}^2s_{12}^2s_{13}^2$
$\Delta_L=0.5$ eV^2	$0.009<A<0.03$	$A<0.0257$	$A<0.04$	$A<0.0257$	-
$\Delta_L=2$ eV^2	$0.0015<A<0.006$	$A<0.06$	$A<0.06$	$A<0.0025$	$A<0.155$
$\Delta_L=6$ eV^2	$0.0022<A<0.008$	$A<0.13$	$A<0.07$	$A<0.002$	$A<0.022$
$\Delta_L=10$ eV^2	$0.0024<A<0.01$	$A<0.13$	$A<0.13$	$A<0.0024$	$A<0.01$

[a]Ref. [1].
[b]Ref. [62].
[c]Ref. [63].
[d]Ref. [64].
[e]Ref. [65].

IV. RESULTS AND DISCUSSIONS

For both the mass spectra discussed in Secs. III A and III B, the survival or transition probabilities for the accelerator and reactor experiments are functions of any two of the mixing angles θ_{12}, θ_{13}, and θ_{23} and one mass-squared difference Δ_L. In a realistic analysis one has to average the probabilities over the L/E distributions of various experiments and fold it with the detector cross sections. We adopt the approach followed in [33] since one mass scale dominance is a good approximation in our case also. As noted in [33], in this limit one can make a one-to-one correspondence between $\sin^2 2\theta$ as obtained from a two-flavor analysis and the angular factor appearing in a three-generation calculation. If we now fix Δm^2 around Δ_L, then from the bound on $\sin^2 2\theta$ at this Δm^2 from two flavor exclusion contours one can constrain the three-generation mixings. The following are the steps adopted by us.

Choosing four representative values of Δ_L, 0.5, 2, 6, and 10 eV^2, we determine the allowed area in the s^2_{13}-s^2_{23} [s^2_{12}-s^2_{13}] parameter space for mass spectrum (i) [(ii)] from the accelerator and reactor constraints presented in Table III.

The probabilities in the atmospheric neutrino case are functions of the three mixing angles θ_{12}, θ_{13}, and θ_{23} and two mass-squared differences Δ_L and Δ_I. The terms involving Δ_L average to 1/2 and do not make an explicit appearance. We determine the allowed area in the s^2_{13}-s^2_{23} [s^2_{12}-s^2_{13}] parameter space for fixed values of s^2_{12} [s^2_{23}] at $\Delta_I \sim 10^{-2}$ eV^2 for mass spectrum (i) [(ii)] solely from the atmospheric neutrino data. We use the sub-GeV Kamiokande result

$$0.48 \leqslant R \leqslant 0.73 \quad (90\% \quad \text{C.L.}), \tag{35}$$

where R is given by Eq. (5).

Next we find the allowed regions of mixing angles admissible from accelerator, reactor, and atmospheric neutrino data and compatible with the solar neutrino oscillations.

Finally the region in the Δ_{14}-$\sin^2 2\theta_{14}$ plane consistent with the solar neutrino data is determined by a χ^2 analysis for both vacuum and MSW oscillations for the case of the mixing of four massive neutrino fields. In this analysis the other three mixing angles are kept in the range permitted from accelerator, reactor, and atmospheric neutrino constraints. For purposes of comparison the two-generation ν_e-ν_s regions are also shown.

Below we discuss the results for each mass spectrum.

A. Accelerator and reactor data

1. Mass spectrum (i)

The constraints on the mixing angles from the various accelerator and reactor neutrino oscillation experiments are given in Table III for values of $\Delta_L = 0.5$, 2.0, 6.0, and 10.0 eV^2. The nonevidence of neutrino oscillations from accelerator and reactor data gives three allowed sectors in the s^2_{13}-s^2_{23} plane: (i) $0 \leqslant s^2_{23} \leqslant 1.0$, large s^2_{13} region; (ii) large s^2_{23}, small s^2_{13} region; (iii) small s^2_{23}, small s^2_{13} region.

These zones are shown in Figs. 2(a)–2(d) for different values of Δ_L. Some of these zones are ruled out when the constraint from the LSND experiment is included.

Figure 2(a) is for $\Delta_L = 0.5$ eV^2. Figure 2(a)(i) gives the allowed area in the first zone mentioned above. In this region the permitted values of the mixing angles are determined by the Bugey and LSND constraints, giving

$$0.994 \lesssim s^2_{13} \lesssim 0.998, \quad 0.32 \lesssim s^2_{23} \lesssim 1.0.$$

Figure 2(a)(ii) displays the admitted zone in the large s^2_{23}, small s^2_{13} region. In this part the most stringent constraints are from Bugey, LSND, and CDHSW, allowing

$$0.0025 \lesssim s^2_{13} \lesssim 0.006, \quad 0.993 \lesssim s^2_{23} \lesssim 1.0.$$

Figure 2(a)(iii) shows that there is no combined allowed region consistent with the constraints from Bugey, CDHSW, and LSND in the small s^2_{23}, small s^2_{13} region.

From Fig. 2(b) which is for $\Delta_L = 2.0$ eV^2, we see that again among the three zones mentioned above only two are consistent with all the accelerator and reactor data plus LSND.

Figure 2(b)(i) gives the large s^2_{13} region. Here most restraining are LSND, E776, and Bugey, giving

$$0.985 \lesssim s^2_{13} \lesssim 0.999, \quad 0.02 \lesssim s^2_{23} \lesssim 1.0.$$

In Fig. 2b(ii) the large s^2_{23}, small s^2_{13} region is displayed. In this zone the most stringent are the constraints from LSND, E776, and CDHSW, giving

$$0.0004 \lesssim s^2_{13} \lesssim 0.0007, \quad 0.985 \lesssim s^2_{23} \lesssim 1.0.$$

The small s^2_{23}, small s^2_{13} region shown in Fig. 2(b)(iii) is ruled out by the combination of LSND, CDHSW, and Bugey.

Figures 2(c) and 2(d) display the situation for $\Delta_L = 6$ and 10 eV^2, respectively. In both these cases one finds no allowed region consistent with all the accelerator and reactor neutrino oscillation data mainly because of the incompatibility of the E776 and LSND results. In region 3, viz., the small s^2_{23} small s^2_{13} region, the E531 constraint is also not consistent with LSND bounds as is shown in Figs. 2(c)(iii) and 2(d)(iii) for $\Delta_L = 6$ and 10 eV^2, respectively.

2. Mass spectrum (ii)

From the constraints given in Table III, one gets three allowed areas of parameter space from nonobservance of neutrino oscillations of all the accelerator and reactor neutrino oscillation experiments apart from LSND. These regions shown in Fig. 3 are (i) $0 \leqslant s^2_{13} \leqslant 1.0$, large s^2_{12} region, (ii) large s^2_{13}, small s^2_{12} region, and (iii) small s^2_{13}, small s^2_{12} region.

When the LSND constraint is included, only two of these zones survive for a narrow range $0.5 \leqslant \Delta_L \leqslant 2$ eV^2.

Figure 3(a) is for $\Delta_L = 0.5$ eV^2. Figure 3(a)(i) gives the large s^2_{12} region. Here most restraining are LSND, E776, and CDHSW, giving the bounds

$$0.99 \lesssim s^2_{12} \lesssim 0.998, \quad 0 \lesssim s^2_{13} \lesssim 0.80.$$

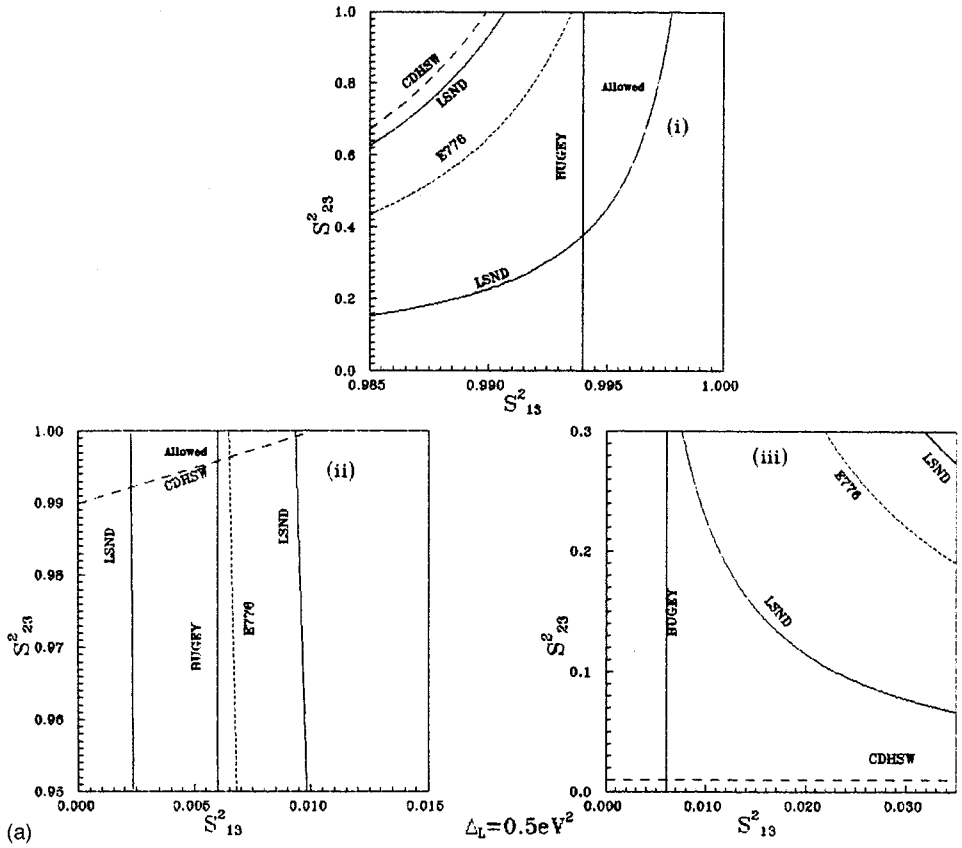

FIG. 2. (a) The allowed region in the s^2_{13}-s^2_{23} plane from accelerator and reactor data for mass spectrum (i) for $\Delta_L=0.5$ eV^2: (i) The $0 \leqslant s^2_{23} \leqslant 1.0$, large s^2_{13} zone. The region between the solid lines is allowed by LSND; the areas to the right of the dashed line marked E776, below the dashed line marked CDHSW, and to the right of the line marked BUGEY are allowed from these experiments, respectively. The region marked ''Allowed'' is consistent with the oscillation signal found in LSND and the null results of other accelerator and reactor experiments. (ii) The high s^2_{23}, low s^2_{13} regime. Here, the region between the solid lines is allowed from LSND, and those to the left of the dashed line marked E776 and solid line marked Bugey are allowed from these experiments. The region above the dashed line marked CDHSW is allowed from it. The zone admitted from all the experiments is marked ''Allowed.'' (iii) The low s^2_{23}, low s^2_{13} region. In this, the areas below the dashed lines marked E776 and CDHSW and to the left of the solid line marked Bugey are allowed. There is no allowed zone in this regime consistent with all the experiments. (b)(i), (ii), and (iii) Same as in (a)(i), (ii), and (iii), respectively, except that these are for $\Delta_L = 2$ eV^2. At this value of Δ_L the constraint from E531 is also relevant. The area above and below the line marked E531 is allowed from this experiment in (b)(ii) and (b)(iii) respectively. (c) Same as in (b) but for $\Delta_L=6$ eV^2. (d) Same as in (b) but for $\Delta_L=10$ eV^2.

In Fig. 3(a)(ii) the large s^2_{13}, small s^2_{12} region is displayed. In this zone no region is simultaneously consistent with the Bugey, LSND, and CDHSW constraints.

Figure 3(a)(iii) shows the small s^2_{12}, small s^2_{13} region where the most stringent constraints come from LSND, Bugey, and E776, giving

$$2.5\times10^{-3} \lesssim s^2_{12} \lesssim 6.5\times10^{-3}, \quad 0.0 \lesssim s^2_{13} \lesssim 0.004.$$

Figure 3(b) is for $\Delta_L=2.0$ eV^2. Figure 3(b)(i) gives the allowed area in the first zone mentioned above. In this region the permitted values of the mixing angles are determined by the E776, CDHSW, and LSND constraints, giving

$$0.985 \lesssim s^2_{12} < 0.998, \quad 0.0 \lesssim s^2_{13} \lesssim 0.98.$$

Figure 3(b)(ii) displays the admitted zone in the large s^2_{13}, small s^2_{12} region. In this part there is no combined allowed region consistent with the constraints from Bugey, CDHSW, and LSND. Figure 3(b)(iii) shows the small s^2_{23}, small s^2_{13} region. In this part the most stringent constraints are from Bugey, LSND, and E776, allowing

$$5\times10^{-4} \lesssim s^2_{12} \lesssim 7\times10^{-4}, \quad 0.0 \lesssim s^2_{13} \lesssim 0.015.$$

As in the case of mass spectrum (i), no allowed region consistent with all the accelerator and reactor neutrino oscillation data is found for $\Delta_L=6$ and 10 eV^2 mainly because of the incompatibility of the E776 and LSND results.

B. Atmospheric neutrino data

The area in the s^2_{13}-s^2_{23} [s^2_{12}-s^2_{13}] parameter space allowed by the sub-GeV Kamiokande data for fixed values of s^2_{12} [s^2_{23}] is shown in Fig. 4 [Fig. 5] for mass spectrum (i) [(ii)]. These plots are drawn by keeping Δ_I fixed at 10^{-2} eV^2 and using Eqs. (5) and (35). We have chosen this form of repre-

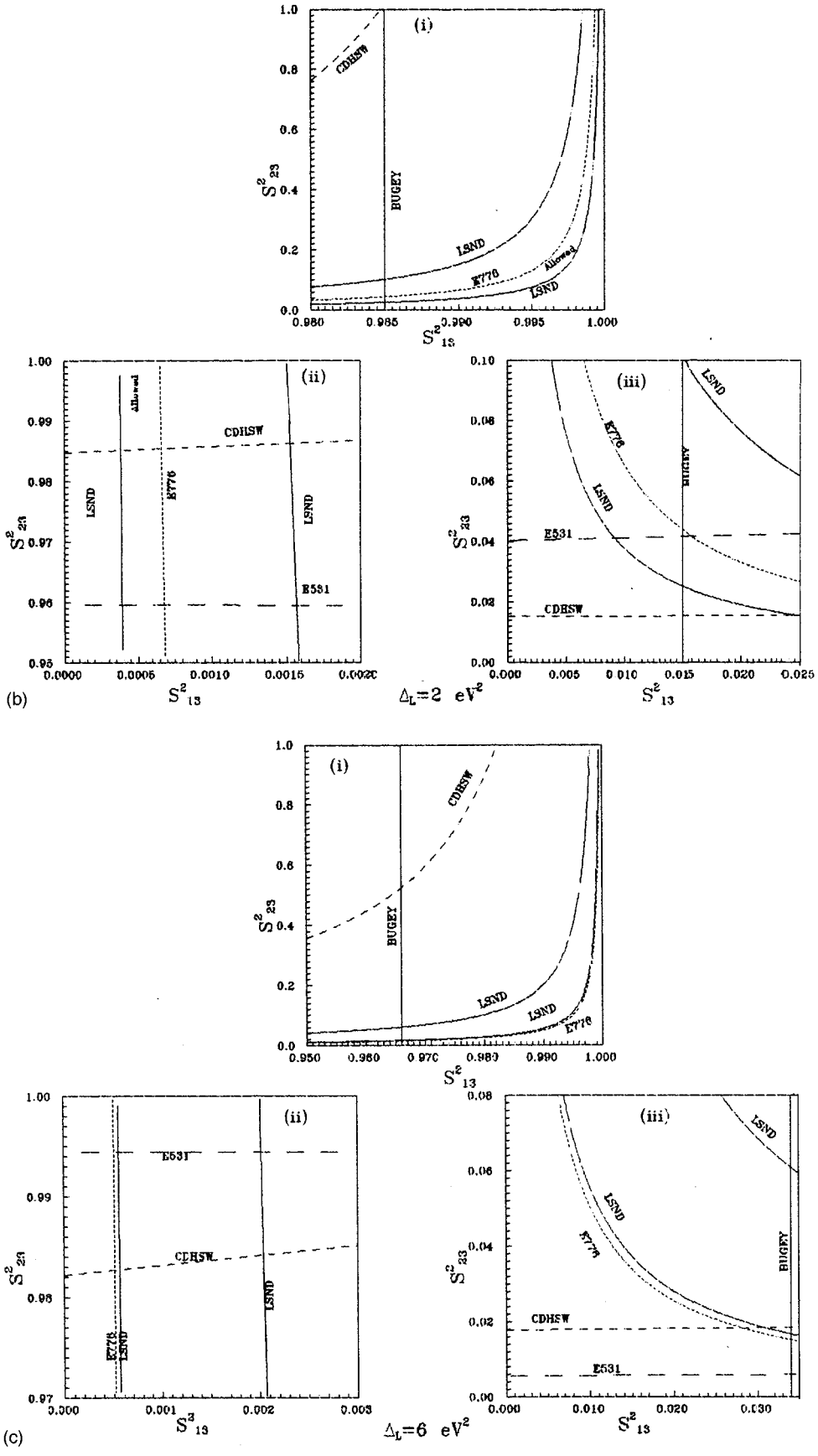

FIG. 2 (*Continued*).

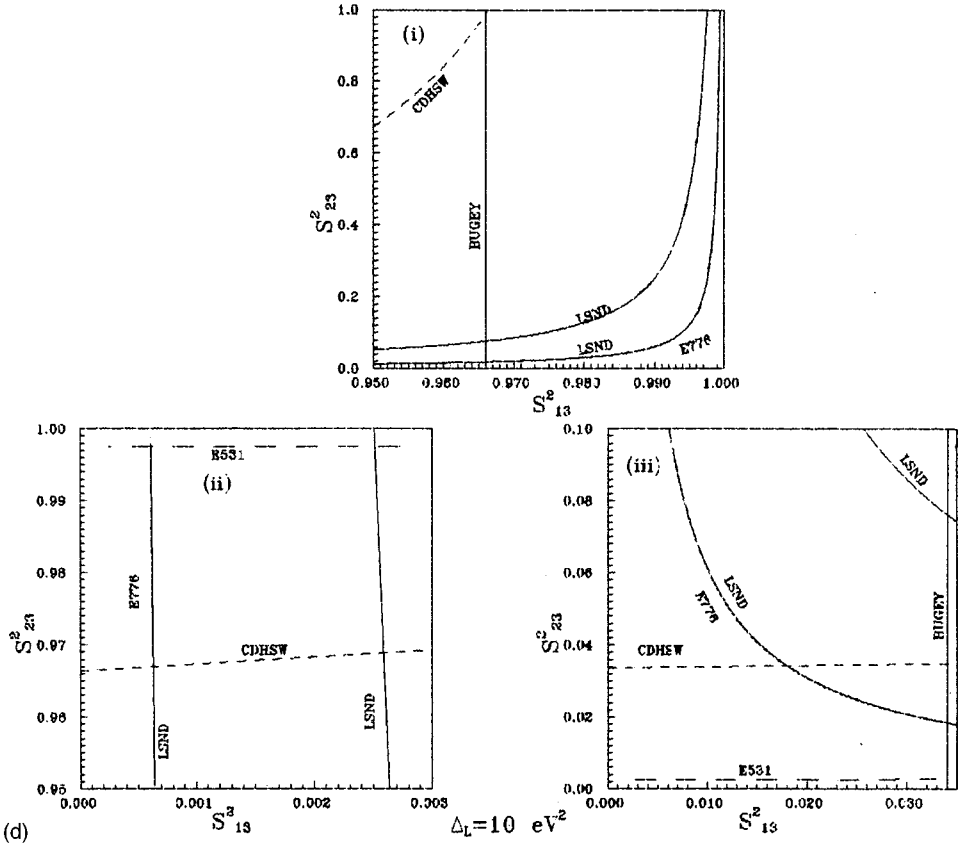

FIG. 2 (*Continued*).

sentation here over the more common mass-squared difference vs mixing angle plots in order to facilitate comparison with the allowed areas from accelerator and reactor data. As mentioned earlier, the Δ_L-dependent short wavelength mode averages out and the results are valid for the entire range 0.5 eV$^2 \leqslant \Delta_L \leqslant 10$ eV^2 considered. The regions shown in Figs. 4 and 5 include genuine three-generation regions where both ν_μ-ν_e and ν_μ-ν_τ channels simultaneously contribute to atmospheric neutrino oscillations in addition to the two-flavor limits. The two-flavor limits are obtained when any two of the mixing angles assume their limiting values of 0 and/or $\pi/2$. The possible two-flavor limits and the corresponding mass scale driving the oscillations are listed in Tables IV(a) and IV(b). Because of the greater latitude allowed by the presence of two mass scales and three mixing angles, there are more choices compared to the one mass scale dominance limit case [55] where the probabilities involve one mass scale and two mixing angles.

C. Combined allowed zone

In this section we discuss the combined allowed zones which are permissible from accelerator and reactor data and atmospheric neutrino anomaly and are compatible with the solar neutrino problem.

1. Mass spectrum (i)

As discussed before, for this mass choice all the accelerator and reactor data including the LSND results give two allowed sectors in the s^2_{13}-s^2_{12} plane for $0.5 \leqslant \Delta_L \leqslant 2$ eV^2. In one of these zones shown in Figs. 2(a)(ii) and 2(b)(ii) for $\Delta_L = 0.5$ and 2 eV^2, respectively, s_{13} stays close to 0 and $s_{23} \rightarrow 1$. From Table IV(a), in this limit ν_e-ν_τ oscillations take place in the atmosphere which drives the ratio of ratios R in a direction opposite to that required. Thus these regions are not expected to be consistent with the atmospheric neutrino data, which is borne out by Fig. 4.

On the other hand, from Fig. 4 for values of s^2_{23} and s^2_{13} lying in the allowed range displayed in 2(a)(i) and 2(b)(i) there are some regions consistent with the atmospheric neutrino data depending on the choice of s^2_{12}. This is the $s^2_{13} \rightarrow 1$ limit. As can be seen from Table IV(a), in this limit ν_μ-ν_τ oscillations occur, which can explain the atmospheric neutrino problem. However, for the solar neutrino survival probability, Eq. (21), the limit $s^2_{13} \rightarrow 1$ would imply that the coefficient of the vital term responsible for the MSW effect, $P_{\rm MSW}$, becomes very small. Consequently $P_{\nu_e \nu_e} \rightarrow 1$ due to the factor s^4_{13} in Eq. (21) contrary to the results from the solar neutrino experiments discussed in Sec. II C. Similarly for the vacuum oscillation probability [Eq. (16)] also one would require that the factor $c^4_{13} c^4_{12}$ multiplying the energy- and Δm^2-dependent term $P_{2\rm vac}$ should not be too small which would again prefer low s^2_{13}. Thus this area is disfavored by the solar neutrino data.

Thus for mass spectrum (i) both regions admitted from the accelerator and reactor constraints are disfavored when

combined with the results from atmospheric and solar neutrino flux measurements. We conclude that mass spectrum (i) cannot reconcile all the existing evidence of neutrino oscillations consistently.

2. Mass spectrum (ii)

The allowed zones for this mass spectrum from accelerator and reactor data were presented in Fig. 3. There are two admitted zones: (i) $0 \leqslant s^2_{13} \leqslant 1.0$, large s^2_{12} region presented in Figs. 3(a)(i) and 3(b)(i) for $\Delta_L = 0.5$ and 2.0 eV^2, respectively; (ii) small s^2_{13}, small s^2_{12} region shown in Figs. 3(a)(iii) and 3(b)(iii).

For Δ_L beyond ~ 2 eV^2 no allowed zones are obtained.

As can be seen from Fig. 5 in the $s_{12} \rightarrow 1$ limit, there is no allowed area from the atmospheric neutrino data irrespective of the choice of s^2_{23}. From Table IV(b), this is the ν_e-ν_τ oscillation region and is not consistent with the atmospheric neutrino data. Thus one is left with the allowed zones of Figs. 3(a)(iii) and 3(b)(iii). This is the $s_{12} \rightarrow 0$, $s_{13} \rightarrow 0$ limit, in which ν_μ-ν_τ oscillations occur for atmospheric neutrinos. The areas shown in Figs. 3(a)(iii) which are simultaneously allowed by the atmospheric neutrino constraint (35) are shown in Fig. 6(a). It is found that for $0.18 \leqslant s^2_{23} \leqslant 0.82$ the whole of the region permitted by the accelerator and reactor constraints is allowed by the atmospheric data. As s^2_{23} is decreased or increased above these limits the allowed region slowly tapers off and beyond $s^2_{23} = 0.17$ on the lower side and $s^2_{23} = 0.83$ on the upper side there is no allowed region consistent with the atmospheric data. Similarly in Fig. 6(b) we show the allowed area of Fig. 3(b)(iii) that is compatible with the atmospheric neutrino constraints for s^2_{23} satisfying $0.18 < s^2_{23} < 0.82$.

In the combined allowed regions of Figs. 6(a) and 6(b) both c_{12} and c_{13} stay close to 1 and thus these regions are compatible with the solar neutrino probabilities.

Thus for this mass spectrum the small s^2_{13}, small s^2_{12} zones presented in Figs. 6(a) and 6(b) are compatible with accelerator, reactor, atmospheric, and solar neutrino results.

D. Solar neutrino data

In this section we determine the allowed area in the Δ_{14}-$\sin^2 2\theta_{14}$ plane for mass spectrum (ii). This exercise is

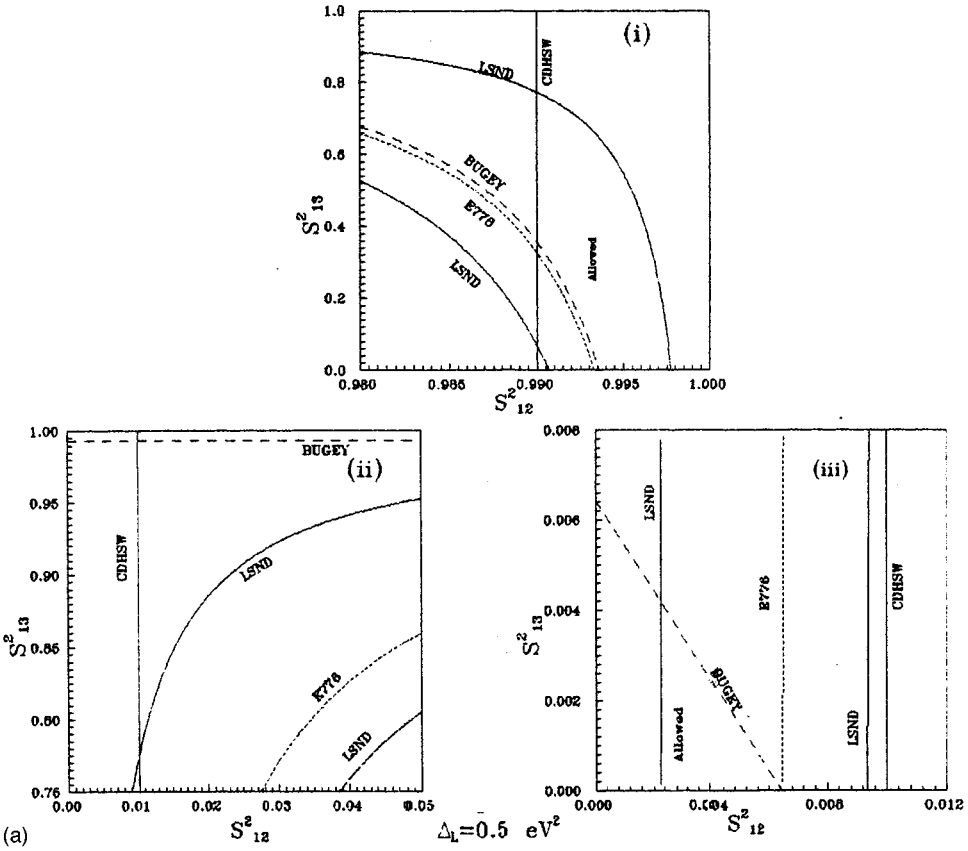

FIG. 3. The allowed region in the s^2_{12}-s^2_{13} plane from accelerator and reactor data for mass spectrum (ii) for $\Delta_L = 0.5$ eV^2: (i) The $0 \leqslant s^2_{13} \leqslant 1.0$, large s^2_{12} region. The area between the solid lines is consistent with LSND, and the areas above the dashed lines marked E776 and Bugey are allowed from these experiments, respectively. The area to the right of the vertical solid line is allowed from CDHSW. The region marked ''Allowed'' is consistent with all the experiments. (ii) The large s^2_{13}, small s^2_{12} region. The area between the solid lines is admitted from LSND while the area to the left of the dashed line marked E776 is allowed from it. The zone above the dashed line marked Bugey is allowed by Bugey and that to the left of the vertical line is allowed from CDHSW. (iii) The small s^2_{13}, small s^2_{12} zone. The region between the solid lines is allowed from LSND. The area below the dashed line marked Bugey is admissible from it while the areas to the left of the solid line marked CDHSW and the dashed line marked E776 are allowed from these experiments, respectively. (b)(i), (ii), and (iii) Same as in (a)(i), (ii), and (iii), respectively, except that these are for $\Delta_L = 2$ eV^2, for which the constraint from E531 is also important in some regions. In (b)(i) the area below [while in (b)(ii) the region to the left] the line marked E531 is allowed.

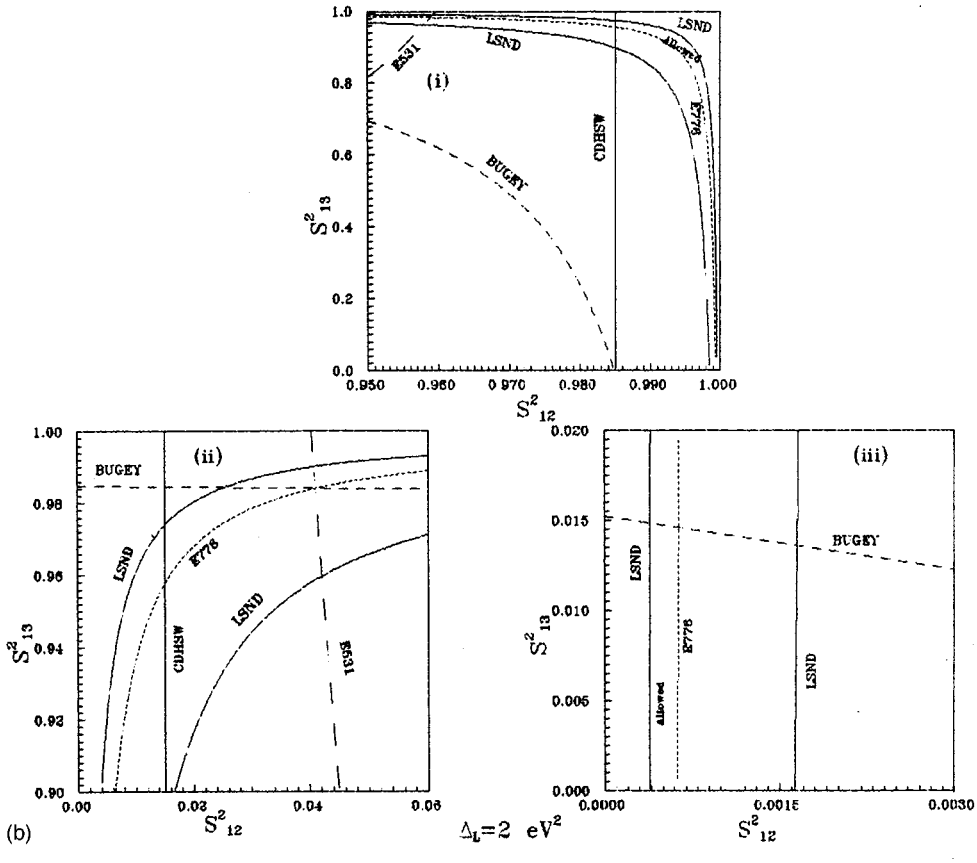

FIG. 3 (*Continued*).

not performed for mass spectrum (i) since it is already disfavored by the combination of all present data. We observe that for mass spectrum (ii) the solar neutrino survival probabilities, Eqs. (16) for the vacuum oscillation case and Eqs. (21) for MSW resonant conversions, depend on Δ_{14} and θ_{14} as well as on combinations of the other three mixing angles θ_{12}, θ_{13}, and θ_{23}. Fixing the values of these mixing angles in the region permitted by the atmospheric and laboratory results (shown in Fig. 6) one can find the allowed area in the Δ_{14}-$\sin^2 2\theta_{14}$ plane using the solar neutrino data.

We have performed a χ^2 analysis of the present solar neutrino data for both the two-generation ν_e-ν_s case as well as for the (3+1) model under consideration for both vacuum oscillations and MSW resonant flavor conversion. The method consists of minimizing the function

$$\chi^2=\sum_{i=1}^{N_{\rm expt}}\left(\frac{R_i^{\rm expt}-R_i^{\rm th}}{\Delta R_i^{\rm expt}}\right)^2, \tag{36}$$

where $R_i^{\rm expt}$ denotes the experimentally observed rate for the ith experiment (given in Table II) and $\Delta R_i^{\rm expt}$ is the corresponding error obtained by combining the statistical and systematic errors in quadrature. $R_i^{\rm th}$ is the theoretically calculated rate for a particular value of Δm^2 and $\sin^2 2\theta$. The parameter values minimizing the χ^2 function defined in Eq. (36) give the best fit to the data.

1. Vacuum oscillations

The possibility of vacuum oscillations of ν_e to active [11,13,14,66,67] and sterile [13,14,68] flavors as a solution to the solar neutrino problem has been pursued by many authors. We have done a two-flavor χ^2 fit to the solar neutrino data of Table II for vacuum oscillations to active and sterile neutrinos. The ν_e survival probability

$$P_{2\rm vac}(E,r,R(t))=1-\sin^2 2\theta\,\sin^2\left[\frac{\pi R(t)}{\lambda}\left(1-\frac{r}{R(t)}\right)\right] \tag{37}$$

is folded with the detector cross sections [69], the solar neutrino fluxes [70], and the neutrino production profile functions [7], integrated over the energy E and the production location r, and averaged over 1 year when compared to the time-averaged data. $R(t)$ in the above is the Sun-Earth distance given by

$$R(t)=R_0\left[1-\epsilon\,\cos\left(2\pi\frac{t}{T}\right)\right], \tag{38}$$

where $R_0=1.49\times10^{13}$ cm is the mean Sun-Earth distance, and $\epsilon=0.0167$ is the ellipticity of the Earth's orbit. t is the time of the year at which the solar neutrino flux is measured and T is 1 year.

Our results are displayed in Table V in which we give the χ^2 minimum and the best-fit values of the parameters for the two-generation vacuum oscillations to active as well as ster-

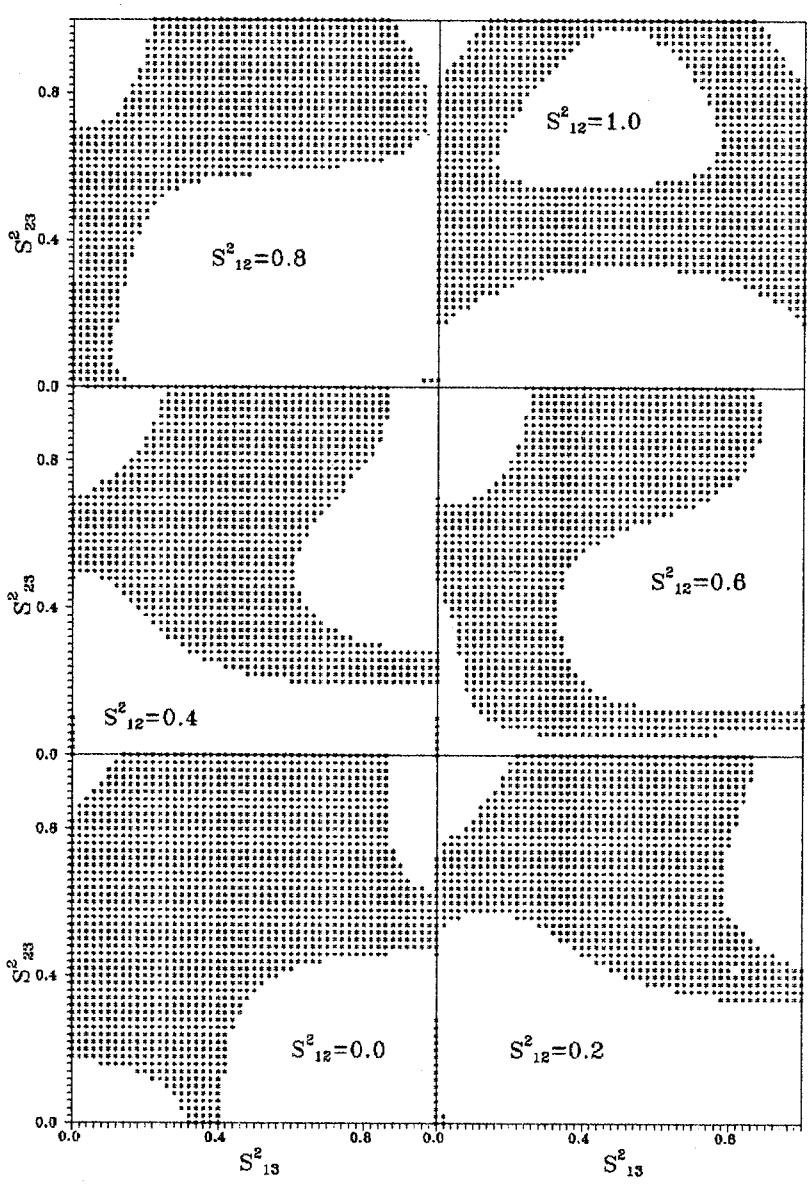

FIG. 4. The allowed areas in the s^2_{13}-s^2_{23} plane from Kamiokande sub-GeV atmospheric neutrino data are shown shaded for various values of s^2_{12} for mass spectrum (i). In these figures $\Delta_I = 10^{-2}$ eV^2.

ile neutrinos. Our results compare well with recent vacuum oscillation analyses in the literature [11,13,14,66]. The small differences can be traced to the use of different input data.

Next we investigate for any possible changes in the χ^2 minimum and the best-fit values of the parameters if instead of the two-flavor probabilities one uses Eq. (33) fixing θ_{12}, θ_{13}, and θ_{23} from the combined allowed zone shown in Fig. 6. We find that for the admissible values of these mixing angles the last two terms of Eq. (33) are negligible and the probability reduces to $P_{\nu_e\nu_e} \approx c^4_{13}c^4_{12}P_{2\mathrm{vac}}$. Any change over the two-flavor ν_e-ν_s case will thus be brought about by the factor $c^4_{13}c^4_{12}$. In addition, in the two-generation case involving just ν_e and ν_s Kamiokande would be sensitive to ν_e's only but here one has the additional possibility of a simultaneous transition to ν_μ's as well as ν_τ's which can interact in the Kamiokande detector by virtue of their neutral current interactions. For the mass spectrum (ii) this contribution is given by

$$P_{\nu_e\nu_\mu} + P_{\nu_e\nu_\tau} \approx c^2_{12}c^2_{13} - c^4_{12}c^4_{13} + (c^2_{12}c^2_{13} - c^4_{12}c^4_{13})P_{2\mathrm{vac}}, \tag{39}$$

where we have neglected a term $2U^2_{e2}U^2_{e3}$ since it is small in the combined allowed region of Fig. 6 from the accelerator, reactor, and atmospheric neutrino data. Scanning over the allowed regions in Fig. 6, the minimum value that the factor $c^4_{13}c^4_{12}$ can take is 0.97. Fixing $c^4_{13}c^4_{12}$ at this value the χ^2 minimum and the best-fit values of the parameters obtained are listed in Table V. The change over the two-generation ν_e-ν_s case is nominal. This is expected because the factor $c^4_{13}c^4_{12}$ is close to 1. Also the contribution to Kamiokande coming from (39) is $\approx 0.015 + 0.015P_{2\mathrm{vac}}$. Thus the maximum contribution from this channel is $\approx 0.03/6$ when $P_{2\mathrm{vac}}$ is 1. The factor of 1/6 comes because the neutral current interactions at the detector are suppressed by this factor compared to the charged current interactions. The 90% C.L. allowed area ($\chi^2 \leq \chi^2_{\mathrm{min}} + 4.61$) for the two-generation sterile

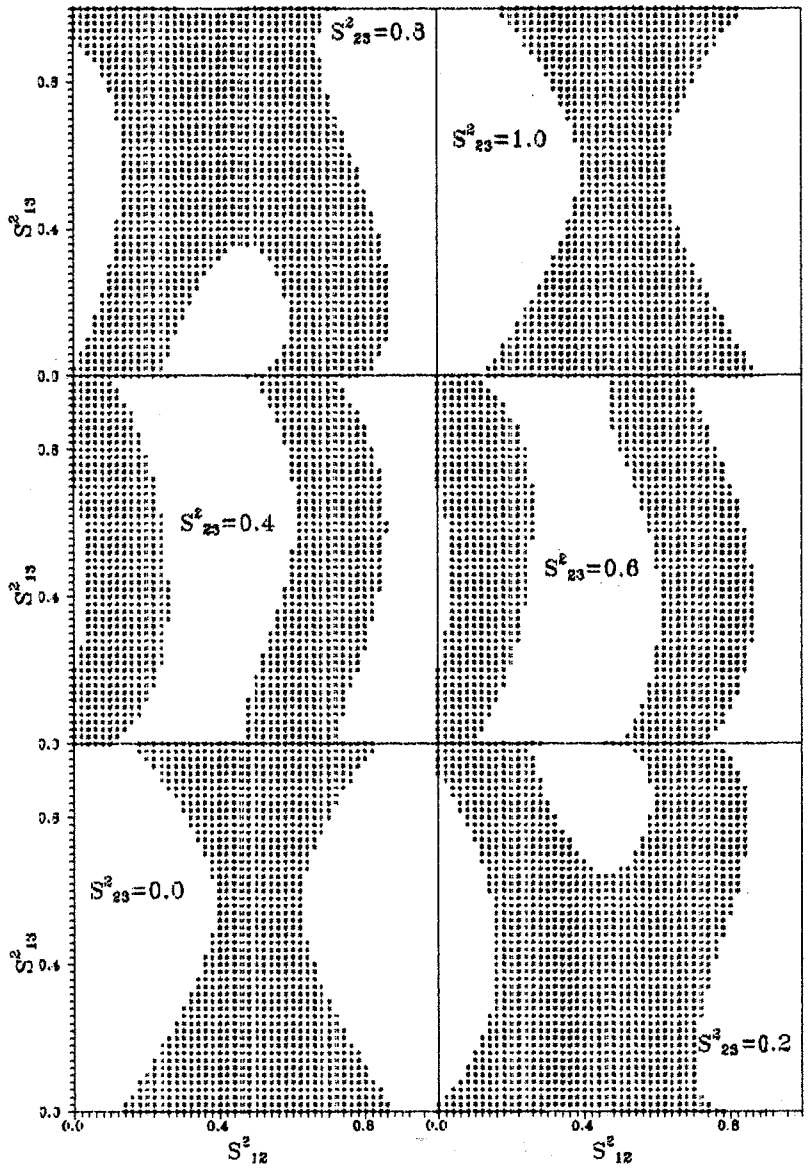

FIG. 5. The allowed areas in the s^2_{12}-s^2_{13} plane from Kamiokande sub-GeV atmospheric neutrino data are shown shaded for various values of s^2_{23} for mass spectrum (ii). In these figures $\Delta_I = 10^{-2}$ eV^2.

neutrino solution and for the (3+1) model under consideration is shown in Fig. 7. In this analysis we have confined ourselves within a particular standard solar model (SSM) [7] and have not considered the theoretical uncertainties and their correlations. It has been shown in [13] that inclusion of theoretical errors does not change the best-fit values and the χ^2 minimum significantly. Only the confidence regions become larger. For our purpose of comparison between the two-flavor ν_e-ν_s case and the four-massive-neutrino model a determination of the χ^2 minimum and the best-fit values suffices.

2. MSW resonant flavor conversion

There are several recent two-flavor MSW analyses of the solar neutrino data [11–13,71–76] which agree well with each other up to small differences due to the different input data and their treatment. We have done a two-flavor fit to the current data for MSW transitions to both active and sterile species. The χ^2 minimum and the best-fit values of parameters obtained are given in Table VI. Instead of numerically integrating the evolution equation we make use of the well-known analytic expression of the two-flavor survival probability of the form (22). This is folded with the energy spectrum and detector cross sections and integrated over the production points. Our algorithm for determining the resonance position and the logarithmic derivative at the resonance point follows the prescription given in [77]. We use the density profiles [60]

$$n = n_0 n_{\rm Avo} \exp\left(\frac{1}{z_0}\frac{-z^2}{(z+b)}\right). \tag{40}$$

The parameter n_0 is 98.8 and 48.4, respectively, for n_e and n_n. $z = r/R_\odot$, and $n_{\rm Avo} = 6.03\times10^{23}/{\rm cm}^3$. b is 0.15 and 0.02, respectively, for n_e and n_n with $z_0 = 0.09$ for both. For the case where oscillation to an active species is considered,

TABLE IV. The possible two-flavor approximations for atmospheric neutrinos.

Angle limit	Equivalent two-flavor mixing	Relevant mass scale
(a) Mass spectrum (i)		
$s_{12}\to 0,\ s_{13}\to 0$	ν_μ-ν_τ	Δ_L
$s_{12}\to 1,\ s_{13}\to 0$	ν_μ-ν_τ	Δ_L
$s_{12}\to 0,\ s_{13}\to 1$	ν_μ-ν_τ	Δ_I
$s_{12}\to 1,\ s_{13}\to 1$	ν_μ-ν_τ	Δ_I
$s_{13}\to 0,\ s_{23}\to 0$	ν_μ-ν_e	Δ_I
$s_{13}\to 0,\ s_{23}\to 1$	ν_e-ν_τ	Δ_I
$s_{13}\to 1,\ s_{23}\to 0$	ν_μ-ν_τ	Δ_I
$s_{13}\to 1,\ s_{23}\to 1$	ν_μ-ν_τ	Δ_I
$s_{12}\to 0,\ s_{23}\to 0$	ν_e-ν_τ	Δ_L
$s_{12}\to 0,\ s_{23}\to 1$	ν_e-ν_μ	Δ_L
$s_{12}\to 1,\ s_{23}\to 0$	ν_e-ν_τ	Δ_L
$s_{12}\to 1,\ s_{23}\to 1$	ν_e-ν_μ	Δ_L
(b) Mass spectrum (ii)		
$s_{12}\to 0,\ s_{13}\to 0$	ν_μ-ν_τ	Δ_I
$s_{12}\to 1,\ s_{13}\to 0$	ν_e-ν_τ	Δ_I
$s_{12}\to 0,\ s_{13}\to 1$	ν_μ-ν_e	Δ_I
$s_{12}\to 1,\ s_{13}\to 1$	ν_e-ν_τ	Δ_I
$s_{13}\to 0,\ s_{23}\to 0$	ν_μ-ν_e	Δ_L
$s_{13}\to 0,\ s_{23}\to 1$	ν_μ-ν_e	Δ_L
$s_{13}\to 1,\ s_{23}\to 0$	ν_μ-ν_τ	Δ_L
$s_{13}\to 1,\ s_{23}\to 1$	ν_μ-ν_τ	Δ_L
$s_{12}\to 0,\ s_{23}\to 0$	ν_e-ν_τ	Δ_L
$s_{12}\to 0,\ s_{23}\to 1$	ν_e-ν_τ	Δ_L
$s_{12}\to 1,\ s_{23}\to 0$	ν_e-ν_τ	Δ_I
$s_{12}\to 1,\ s_{23}\to 1$	ν_e-ν_τ	Δ_I

only n_e appears in the expression for the probabilities. For this case we have compared the χ^2 minimum obtained using the SSM densities given in a tabular form in [7] with that obtained by using the density profile of Eq. (40). The results are almost the same.

Next we determine the χ^2 minimum and the best-fit values of the parameters for the model consisting of four massive neutrinos under consideration for which we use the probability (34). Compared to the two-generation scenario the following points of qualitative difference are there in our case.

The survival probability given in Eq. (34) depends on three additional mixing angles θ_{12}, θ_{13}, and θ_{23}.

The resonance condition and the mixing angle in matter are now determined by $n_{\rm eff}$ given by Eq. (19) which depends on the mixing angles θ_{12} and θ_{13}.

In earlier studies of the three-generation MSW effect, conversion between active species was considered and hence the term involving the neutron density was absent and the jump probability retained its two generation form [30,33]. Here, because of the asymmetric interaction between the active and the sterile species, the jump probability between the first and fourth states is also affected by mixing with the second and third states.

Our aim is to see whether these can make any quantitative difference in the two-generation ν_e-ν_s confidence regions and best-fit values for the allowed values of the mixing angles θ_{12}, θ_{13}, and θ_{23}, consistent with accelerator, reactor, and atmospheric data, depicted in Fig. 6.

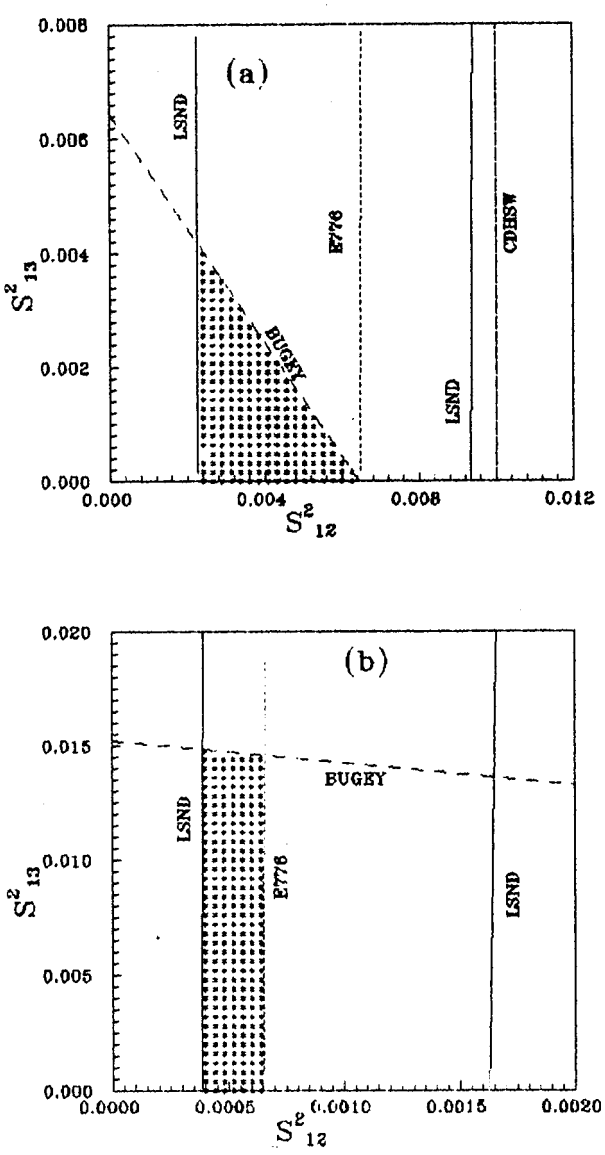

FIG. 6. The combined allowed area consistent with the accelerator, reactor, atmospheric, and solar neutrino results are shown shaded in (a) for $\Delta_L = 0.5$ eV^2 and (b) for $\Delta_L = 2$ eV^2. In the above figures $\Delta_I = 10^{-2}$ eV^2 and $0.18 < s^2_{23} < 0.82$.

As before, for the allowed zones of Fig. 6 the last two terms in Eq. (34) are negligible and one has $P_{\nu_e\nu_e} \approx c^4_{12}c^4_{13}P_{\rm MSW}$. In the allowed region of Fig. 6 the minimum possible value of $c^4_{12}c^4_{13}$ is 0.97. With this choice

TABLE V. The $\chi^2_{\rm min}$ and the best-fit values of Δm^2 and $\sin^2 2\theta$ for vacuum oscillation of solar neutrinos. Note that for the four-generation case $\Delta m^2 \equiv \Delta_{14}$ and $\sin^2 2\theta \equiv \sin^2 2\theta_{14}$.

	Two generation (active)	Two generation (sterile)	Four generation $c^4_{13}c^4_{12} = 0.97$
$\chi^2_{\rm min}$	3.0	8.15	8.07
Δm^2 [10^{-11} eV^2]	6.1	7.87	7.89
$\sin^2 2\theta$	0.93	0.81	0.80

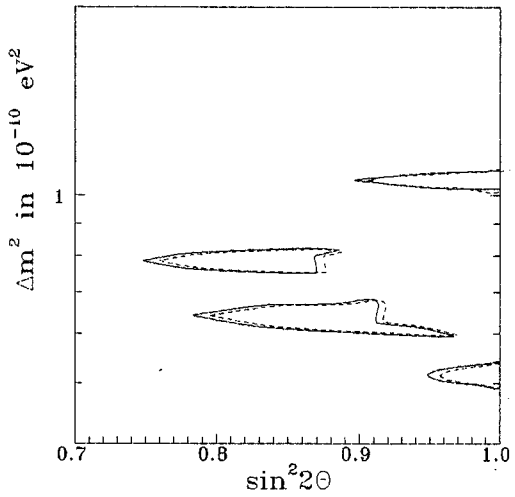

FIG. 7. The 90% C.L. region in the Δm^2-$\sin^2 2\theta$ plane for the vacuum oscillation solution to the solar neutrino problem. The dashed line is for the two-generation ν_e-ν_s solution while the solid line is for the four-neutrino case with $c_{12}^4 c_{13}^4 = 0.97$. Note that for the four-neutrino case $\Delta m^2 \equiv \Delta_{14}(\Delta_S)$ and $\sin^2 2\theta \equiv \sin^2 2\theta_{14}$.

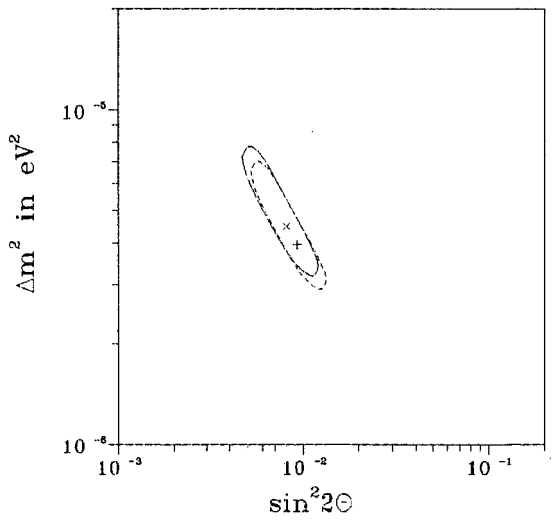

FIG. 8. The 90% C.L. region in the Δm^2-$\sin^2 2\theta$ plane for the MSW solution to the solar neutrino problem. The dashed contour is for the two-generation ν_e-ν_s solution while the solid contour is for the four-neutrino case with $c_{12}^4 c_{13}^4 = 0.97$. The ''+'' denotes the best-fit solution in the first case while ''×'' denotes that in the second. For the four-neutrino situation $\Delta m^2 \equiv \Delta_{14}$ and $\sin^2 2\theta \equiv \sin^2 2\theta_{14}$.

$n_{\rm eff}$ of Eq. (19) differs at most by 7% from the profile of $n_e - \frac{1}{2} n_n$, which is relevant for the two-flavor sterile neutrino solution, in the region of neutrino production in the Sun. Here $(1/n_{\rm eff})(dn_{\rm eff}/dz)$ differs from the logarithmic derivative relevant for the two-generation ν_e-ν_s case by $\approx$5% except at very interior points in the sun. The best-fit values and the χ^2 minimum obtained are presented in Tables VI(a) and VI(b) for the small-angle and large-angle solutions, respectively. The large-angle solution is disfavored for both the two-generation ν_e-ν_s case as well as for our model consisting of four neutrinos for the allowed values of the other mixing angles from accelerator, reactor, and atmospheric neutrino data. The 90% C.L region for the two-generation and the four-neutrino cases is shown in Fig. 8. The change is not significant. The large-angle region is not present in both cases at 90% C.L.

As in the vacuum oscillation case, we have not taken any theory errors or their correlations into account. Further we have not considered the day-night effect in the Kamiokande data and the effect of neutrino regeneration in the Earth. In this respect our two-generation MSW studies are similar to the recent analysis in [11] and our results compare well with them. Since our aim is a comparative study between the two- and four-neutrino models, these omissions are not important for us.

E. Future experiments

The mass spectrum (ii) discussed in this paper reduces to the three-generation case discussed in [29] in the limit $\theta_{14} \to 0$. The implications of the allowed areas shown in Fig. 6 for the mass spectrum (ii) for future short base line experiments like CHORUS and NOMAD and the proposed long base line experiments have been discussed in [29] where it has been shown that with their projected sensitivity CHORUS and NOMAD will not be able to probe these zones but some of the long base line experiments might.

In this article we discuss whether the future solar neutrino experiment SNO will be able to differentiate between the two-generation ν_e-ν_s case and this four-generation scenario. The SNO heavy water experiment [78] will probe, in addition to neutrino electron scattering, neutral and charged current deuteron disintegration reactions initiated by neutrinos via the reactions

$$\nu_e + d \to p + p + e^- \quad \text{(CC absorption)}, \tag{41}$$

$$\nu_x + d \to p + n + \nu_x \quad \text{(NC dissociation)}, \tag{42}$$

where x can be e, μ, or τ. The charged current event rate ($R_{\rm CC}$) and the neutral current event rate ($R_{\rm NC}$) are given in the presence of neutrino flavor conversion by the following expressions.

TABLE VI. The $\chi^2_{\rm min}$ and the best-fit values of Δm^2 and $\sin^2 2\theta$ for the MSW solution to the solar neutrino problem. Note that for the four-generation case $\Delta m^2 \equiv \Delta_{14}$ and $\sin^2 2\theta \equiv \sin^2 2\theta_{14}$.

	Two generation (active)	Two generation (sterile)	Four generation $c_{13}^4 c_{12}^4 = 0.97$
	(a) Small-angle region		
$\chi^2_{\rm min}$	0.26	2.15	2.13
Δm^2 [10^{-6} eV^2]	5.1	3.95	4.48
$\sin^2 2\theta$	7.8×10^{-3}	9.2×10^{-3}	8.1×10^{-3}
	(b) Large-angle region		
$\chi^2_{\rm min}$	2.58	9.68	9.83
Δm^2 [10^{-5} eV^2]	1.8	1.18	1.5
$\sin^2 2\theta$	0.725	0.793	0.802

1. ν_e-$\nu_\mu(\nu_\tau)$ transition

In this case,

$$R_{\rm CC}=R_{\rm CC}^{\rm SSM}\frac{\int F(E)\sigma_{\rm CC}(E)P_{\nu_e\nu_e}(E)dE}{\int F(E)\sigma_{\rm CC}(E)dE}, \tag{43}$$

$$R_{\rm NC}=R_{\rm NC}^{\rm SSM}\frac{\int F(E)\sigma_{\rm NC}(E)[P_{\nu_e\nu_e}(E)+P_{\nu_e\nu_\mu}(E)]dE}{\int F(E)\sigma_{\rm NC}(E)dE}. \tag{44}$$

Since $P_{\nu_e\nu_e}+P_{\nu_e\nu_\mu}=1$ for two flavors, $R_{\rm NC}=R_{\rm NC}^{\rm SSM}$. This conclusion is valid for three active flavors as well. A simple-minded estimate neglecting the detector efficiency and energy resolutions gives $R_{\rm CC}/R_{\rm CC}^{\rm SSM}\approx 0.3$, using the current best-fit small-angle MSW parameters from Table VI(a).

2. ν_e-ν_s transition (two flavor)

$R_{\rm CC}$ is given by Eq. (43) while $R_{\rm NC}$ is

$$R_{\rm NC}=R_{\rm NC}^{\rm SSM}\frac{\int F(E)\sigma_{\rm NC}(E)P_{\nu_e\nu_e}(E)dE}{\int F(E)\sigma_{\rm NC}(E)dE}. \tag{45}$$

Evaluating this quantity with the current best-fit parameters (the small-angle MSW solution) for oscillations to sterile neutrinos, $R_{\rm NC}/R_{\rm NC}^{\rm SSM}$ is 0.35 while $R_{\rm CC}/R_{\rm CC}^{\rm SSM}$ is 0.346. Thus $(R_{\rm CC}/R_{\rm CC}^{\rm SSM})/(R_{\rm NC}/R_{\rm NC}^{\rm SSM})\approx 1$ modulo the small differences between $\sigma_{\rm CC}$ and $\sigma_{\rm NC}$.

3. Mixing of four neutrinos

$R_{\rm CC}$ continues to be given by Eq. (43) but $R_{\rm NC}$ is

$$R_{\rm NC}=R_{\rm NC}^{\rm SSM}\frac{\int F(E)\sigma_{\rm NC}(E)[P_{\nu_e\nu_e}(E)+P_{\nu_e\nu_\mu}(E)+P_{\nu_e\nu_\tau}(E)]dE}{\int F(E)\sigma_{\rm NC}(E)dE}. \tag{46}$$

This is qualitatively different from the two-generation ν_e-ν_s case because of contributions in the neutral current event rate from ν_μ and ν_τ. However, for values of the parameters from Table VI(a), the quantitative difference is not significant and one gets $R_{\rm NC}/R_{\rm NC}^{\rm SSM}$ is 0.37 while $R_{\rm CC}/R_{\rm CC}^{\rm SSM}$ is 0.34 and $(R_{\rm CC}/R_{\rm CC}^{\rm SSM})/(R_{\rm NC}/R_{\rm NC}^{\rm SSM})=0.93$. Thus the presence of two other active neutrino states does not make much of a difference. This is expected because for our model the allowed values of the mixings angles θ_{12} and θ_{13} are very small. We conclude that although future solar neutrino experiments can distinguish in principle between the two-neutrino and four-neutrino mixing models, given the present experimental constraints on parameters these differences are not appreciable.

V. SUMMARY AND CONCLUSIONS

We have performed a combined analysis of the accelerator, reactor, atmospheric, and solar neutrino data in a four-neutrino framework introducing a sterile neutrino ν_s. In such a scenario there are in general six mass-squared differences, three of which are independent, and six mixing angles, neglecting CP violation in the lepton sector. We assume that ν_s mixes only with ν_e, thus reducing the number of mixing angles to four: θ_{12}, θ_{13}, θ_{23}, and θ_{14}. Fixing the three independent Δm^2's around the ranges suitable for LSND, atmospheric, and solar neutrino oscillations, we determine the mixing angles consistent with all the experimental constraints. We consider a picture where Δ_{14} is fixed in the solar neutrino range (either MSW or vacuum oscillation). Then one can think of two different mass spectra (see Fig. 1) for the remaining five Δm^2's: mass spectrum (i), in which two Δm^2's are in the atmospheric range and the other three in the LSND range, and mass spectrum (ii), where one Δm^2 is in the atmospheric range and the remaining four in the LSND range. For both cases one can parametrize the mixing matrix in such a way that the probabilities for the accelerator and reactor experiments are functions of only two mixing angles and one independent Δm^2, viz., Δ_L. Fixing Δ_L around 0.5, 2, 6, and 10 eV^2 we map out the allowed zone in the $\sin^2\theta_{13}$-$\sin^2\theta_{23}$ [$\sin^2\theta_{12}$-$\sin^2\theta_{13}$] plane for the mass spectrum (i) [(ii)]. Using the atmospheric neutrino constraint the above area can be further restricted and the permissible ranges for the remaining mixing angle can be determined. Next we examine whether the combined allowed area thus obtained is compatible with the solar neutrino results.

In general for both mass spectra the following picture emerges: The accelerator and reactor experiments including LSND give two allowed sectors of relevant mixing angles for $0.5\leqslant\Delta_L\leqslant 2$ eV^2. In one of these zones a simultaneous solution to the atmospheric anomaly is possible. For mass spectrum (i) this zone is disfavored by the solar neutrino data whereas for mass spectrum (ii) a narrow region is simultaneously compatible with the Kamiokande atmospheric neutrino data and the solar neutrino results. Thus our analysis shows that mass spectrum (i) is eliminated by combining simultaneously all present data on neutrino oscillations.

Finally, we determine the allowed area in the Δ_{14}-$\sin^2 2\theta_{14}$ plane from the solar neutrino data for mass spectrum (ii), which is favored by the combination of the current data. In a four-neutrino framework the solar neutrino probabilities are in addition functions of three other mixing angles, θ_{12}, θ_{13}, and θ_{23}. Taking these from the combined allowed zone, the possible changes of the allowed area in the Δ_{14}-$\sin^2 2\theta_{14}$ plane are determined. No significant changes over the two-generation ν_e-ν_s case is found. The small-mixing angle MSW solution continues to give the best fit to the data with a χ^2 minimum of 2.13 for two degrees of freedom.

In analyzing the accelerator and reactor data we have used

the two-flavor plots presented by the experimental groups adopting the approach followed in [33] since one mass scale dominance is a good approximation. A rigorous reanalysis of the raw data in the one mass scale limit of the three-generation picture is performed in [34]. The results that we have obtained using the two-flavor plots are more or less in agreement with their analysis. For atmospheric neutrinos we have gone beyond the one mass scale limit and explored the effects of the presence of all three mixing angles and two mass scales. This scenario offers some new solution regions over that obtained in the one mass scale dominance limit. A detailed analysis of the atmospheric neutrino problem in this framework including matter effects and the multi-GeV Kamiokande data will be presented elsewhere [79].

Massive neutrinos are known to be important in supernova r-process nucleosynthesis and the effect of two-generation mixing on r-process nucleosyntheis has been considered in [80]. It has been shown in [37] that in the one mass scale dominance limit the results of two-neutrino mixing can be applied to the three-generation case. For mass spectrum (i) only Δ_{13} is in the relevant range of resonant flavor conversion in the post core-bounce supernova environment and hence the one mass scale dominance limit is applicable and the results of two-generation studies continue to remain valid. However, for the favored mass spectrum (ii) two of the mass-squared differences $\Delta_{12} \approx \Delta_{13}$ are in the range suitable for resonant flavor conversion during r-process nucleosynthesis and ν_e can resonate with two neutrino flavors. Thus, in this case, the two-neutrino results might not be directly applicable. This point is also raised in [37] and merits further scrutiny.

Both mass spectra considered are consistent with the cold plus hot dark matter scenario of structure formation with three almost degenerate [mass spectrum (i)] and two almost degenerate [mass spectrum (ii)] neutrinos in the eV mass range [3,81]. For certain choices of the cosmological parameters such scenarios can provide a better fit to the existing data than the single-neutrino case.

In conclusion, we would like to mention that though a three-flavor mixing scheme cannot accommodate the three hierarchically different mass ranges required for LSND, atmospheric, and solar neutrino oscillations, introducing an additional sterile neutrino, there is more than one possible mass spectrum. We have considered two different mass spectra and have shown that one of these is favored by the current data on neutrino oscillations whereas the other is ruled out by the combination of all data at 90% C.L. Our analysis assumes that the solar neutrino oscillation is driven mainly by ν_e-ν_s transitions. If this scenario is confirmed by the future solar neutrino experiments and the other experimental inputs do not change significantly as more data accumulates, then the case for a fourth sterile neutrino will become very compelling.

ACKNOWLEDGMENTS

The author is indebted to Amitava Raychaudhuri for many useful suggestions, discussions, a careful scrutiny of the manuscript, and encouragement at every stage of this work. She also wishes to thank S.T. Petcov for fruitful discussions and Kamales Kar for discussions and help. Financial support from the Council of Scientific and Industrial Research, India is acknowledged.

[1] C. Athanassopoulos *et al.*, Phys. Rev. Lett. **75**, 2650 (1995); W. C. Louis, in *Neutrino 94*, Proceedings of the 16th International Conference on Neutrino Physics and Astrophysics, Ei'lat, Israel, edited by A. Dar *et al.* [Nucl. Phys. B (Proc. Suppl.) **38**, 229 (1995)].

[2] J. E. Hill, Phys. Rev. Lett. **75**, 2654 (1995). Here the data of [1] were interpreted to be consistent with no neutrino oscillation.

[3] J. R. Primack *et al.*, Phys. Rev. Lett. **74**, 2160 (1995).

[4] The recent results of the LSND Collaboration, C. Athanassopoulos *et al.*, Phys. Rev. C **54**, 2685 (1996), including the data taken in 1995, corroborate their initial results.

[5] G. Raffelt and J. Silk, Phys. Lett. B **366**, 429 (1996); G. M. Fuller, J. R. Primack, and Y. Z. Qian, Phys. Rev. D **52**, 1288 (1995); D. O. Caldwell and R. N. Mohapatra, Phys. Lett. B **354**, 371 (1995).

[6] J. N. Bahcall and M. H. Pinsonneault, Rev. Mod. Phys. **64**, 885 (1992); S. Turck-Chiéze and I. Lopes, Astrophys. J. **408**, 347 (1993).

[7] J. N. Bahcall and M. H. Pinsonneault, Rev. Mod. Phys. **67**, 1 (1995).

[8] N. Hata and P. Langacker, Phys. Rev. D **47**, 2220 (1993); J. N. Bahcall, Phys. Lett. B **338**, 276 (1994); W. Kwong and S. P. Rosen, Phys. Rev. Lett. **73**, 369 (1994); S. Parke, *ibid.* **74**, 839 (1995).

[9] S. M. Bilenky and B. M. Pontecorvo, Sov. Phys. Usp. **20**, 776 (1977).

[10] L. Wolfenstein, Phys. Rev. D **34**, 969 (1986); S. P. Mikheyev and A. Yu. Smirnov, Sov. J. Nucl. Phys. **42**, 913 (1985); Nuovo Cimento C **9**, 17 (1986).

[11] J. N. Bahcall and P. I. Krastev, Phys. Rev. D**53**, 4211 (1996).

[12] P. I. Krastev and S. T. Petcov, Nucl. Phys. **B449**, 605 (1995).

[13] E. Calabresu *et al.*, Astropart. Phys. **4**, 159 (1995).

[14] N. Hata, University of Pennsylvania Report No. UPR-0605T, 1994 (unpublished); P. I. Krastev and S. T. Petcov, Phys. Rev. Lett. **72**, 1960 (1994).

[15] K. S. Hirata *et al.*, Phys. Lett. B **280**, 146 (1992).

[16] Y. Fukuda *et al.*, Phys. Lett. B **335**, 237 (1994).

[17] D. Casper *et al.*, Phys. Rev. Lett. **66**, 2561 (1991); R. Becker-Szendy *et al.*, Phys. Rev. D **46**, 3720 (1992).

[18] Ch. Berger *et al.*, Phys. Lett. B **227**, 489 (1989).

[19] M. Aglietta *et al.*, Europhys. Lett. **8**, 611 (1989).

[20] M. Goodman *et al.*, in *Neutrino 94* [1], p. 337.

[21] The usage of the ''ratio of ratios'' R as a valid indicator of the neutrino anomaly has been recently critically examined. See G. L. Fogli and E. Lisi, Phys. Rev. D **52**, 2775 (1995).

[22] X. Shi, D. Schramm, and B. Fields, Phys. Rev. D **48**, 2563 (1993).

[23] C. J. Copi, D. N. Schramm, and M. S. Turner, Phys. Rev. Lett. **75**, 3981 (1995); N. Hata *et al.*, *ibid.* **75**, 3977 (1995).

[24] A chronological discussion on the bounds obtained by different groups and the various uncertainties involved can be found, e.g., in S. Sarkar, Rep. Prog. Phys. 59, 1 (1996).
[25] P. J. Kernan and S. Sarkar, Phys. Rev. D **54**, 3681 (1996).
[26] R. Foot and R. R. Volkas, Phys. Rev. Lett. **75**, 4350 (1995). Here the big bang nucleosynthesis bounds on mixing with sterile species are reexamined and it is shown that large mixings with sterile neutrinos are allowed if the relic neutrino asymmetry is large.
[27] K. S. Babu, J. C. Pati, and F. Wilczek, Phys. Lett. B **359**, 351 (1995); **364**, 251(E) (1995); S. M. Bilenky, A. Bottino, C. Giunti, and C. W. Kim, *ibid.* **356**, 273 (1995); H. Minakata, *ibid.* **356**, 61 (1995).
[28] H. Minakata, Phys. Rev. D **52**, 6630 (1995).
[29] S. Goswami, K. Kar, and A. Raychaudhuri, Int. J. Mod. Phys A (to be published).
[30] A. S. Joshipura and P. I. Krastev, Phys. Rev. D **50**, 3484 (1994).
[31] A. Acker, A. B. Balantekin, and F. Loreti, Phys. Rev. D **49**, 328 (1994).
[32] M. Narayan *et al.*, Phys. Rev. D **53**, 2809 (1996).
[33] G. L. Fogli, E. Lisi, and D. Montanino, Phys. Rev. D **49**, 3626 (1994).
[34] G. L. Fogli, E. Lisi, and G. Scioscia, Phys. Rev. D **52**, 5334 (unpublished) (1995).
[35] O. Yasuda and H. Minakata, Report No. TMUP-HEL-9604, 1996 (unpublished).
[36] G. L. Fogli, E. Lisi, and D. Montanino, Astropart. Phys. **4**, 177 (1995).
[37] C. Cardall and G. M. Fuller, Phys. Rev. D **53**, 4421 (1996).
[38] O. Yasuda, Report No. TMUP-HEL-9603, hep-ph/9602342, 1996 (unpublished).
[39] J. J. Gomez-Cadenas and M. C. Gonzalez-Garcia, Z. Phys. C **71**, 443 (1996).
[40] S. M. Bilenky *et al.*, Phys. Rev. D **54**, 4432 (1996).
[41] N. Okada and O. Yasuda, Report No. TMUP-HEL-9605, hep-ph/9606411, 1996 (unpublished).
[42] L. Bento and J. W. F. Valle, Phys. Lett. B **264**, 373 (1991); J. Peltoniemi, A. Yu. Smirnov, and J. W. F. Valle, *ibid.* **286**, 321 (1992); J. Peltoniemi *et al.*, *ibid.* **298**, 383 (1993); D. O. Caldwell and R. N. Mohapatra, Phys. Rev. D **48**, 3259 (1993).
[43] See, for example, E. Ma and J. Pantaleone, Phys. Rev. D **52**, 3763 (1995); E. Ma and P. Roy, *ibid.* **52**, R4780 (1995); E. J. Chun, Anjan S. Joshipura, and A. Yu. Smirnov, Phys. Lett. B **357**, 608 (1995); N. Okada, Report No. hepph/9606221, 1996 (unpublished).
[44] For reviews see L. Oberauer and F. Von. Feilitzsch, Rep. Prog. Phys. **55**, 1093 (1992); S. M. Bilenky and S. T. Petcov, Rev. Mod. Phys. **59**, 671 (1987).
[45] D. Saltzberg, Phys. Lett. B **355**, 499 (1995).
[46] B. T. Cleveland *et al.*, in *Neutrino 94* [1], p. 47.
[47] K. S. Hirata *et al.*, Phys. Rev. D **44**, 2241 (1991); Y. Suzuki *et al.*, in *Neutrino 94* [1], p. 54.
[48] P. Anselman *et al.*, Phys. Lett. B **285**, 376 (1992); **327**, 377 (1994).
[49] A. I. Abazov *et al.*, Phys. Rev. Lett. **67**, 3332 (1991); G. Nico *et al.*, in *Proceedings of the XXVII International Conference on High Energy Physics (Glasgow)*, edited by P. J. Bussey and I. G. Knowles (Institute of Physics Publishing, Bristol, 1995), p. 965.
[50] V. Barger, *et al.*, Phys. Lett. **93B**, 195 (1980); J. Phys. G **6**, L165 (1980); V. Barger, K. Whisnant, and R. J. N. Phillips, Phys. Rev. D **22**, 1636 (1980); A. De Rujula *et al.*, Nucl. Phys. **B168**, 54 (1980).
[51] A. Acker, J. G. Learned, S. Pakvasa, and T. J. Weiler, Phys. Lett. B **298**, 149 (1993).
[52] V. Barger and K. Whisnant, Phys. Lett. B **209**, 365 (1988).
[53] G. Barr, T. K. Gaisser, and T. Stanev, Phys. Rev. D **39**, 3532 (1989); T. K. Gaisser, T. Stanev, and G. Barr, *ibid.* **38**, 85 (1988).
[54] M. Nakahata *et al.*, J. Phys. Soc. Jpn. **55**, 3786 (1986).
[55] J. Pantaleone, Phys. Rev. D **49**, R2152 (1994).
[56] E. D. Carlson, Phys. Rev. D **34**, 1454 (1986).
[57] E. Akhmedov, P. Lipari, and M. Lusignoli, Phys. Lett. B **300**, 128 (1993).
[58] G. L. Fogli *et al.*, Report No. IASSNS-AST 96/41, 1996 (unpublished).
[59] T. K. Kuo and J. Pantaleone, Rev. Mod. Phys. **61**, 937 (1989) and references therein; See also D. Harley, T. K. Kuo, and J. Pantaleone, Phys. Rev. D **47**, 4059 (1993). Recent studies include G. L. Fogli, E. Lisi, and D. Montanino, *ibid.* **54**, 2048 (1996).
[60] V. Barger *et al.*, Phys. Rev. D **43**, R1759 (1991).
[61] S. T. Petcov, Phys. Lett. B **200**, 373 (1988); Nucl. Phys. **B13**, 527 (1990).
[62] B. Achkar *et al.*, Nucl. Phys. **B434**, 503 (1995).
[63] F. Dydak *et al.*, Phys. Lett. B **314**, 281 (1984).
[64] L. Borodovsky *et al.*, Phys. Rev. Lett. **68**, 274 (1992).
[65] N. Ushida *et al.*, Phys. Rev. Lett. **57**, 2897 (1986).
[66] Z. G. Berezhiani and A. Rossi, Phys. Rev. D **51**, 5229 (1995); Phys. Lett. **B367**, 219 (1996).
[67] P. I. Krastev and S. T. Petcov, Phys. Rev. D **53**, 1665 (1996).
[68] V. Barger *et al.*, Phys. Rev. D **43**, 1110 (1991); Phys. Rev. Lett. **65**, 3084 (1990); **69**, 3135 (1992); A. Acker, S. Pakvasa, and J. Pantaleone, Phys. Rev. D **43**, 1754 (1991).
[69] J. N. Bahcall and R. K. Ulrich, Rev. Mod. Phys. **60**, 297 (1988).
[70] J. N. Bahcall, *Neutrino Astrophysics* (Cambridge University Press, Cambridge, England, 1989).
[71] N. Hata and P. Langacker, Phys. Rev. D **50**, 632 (1994); **52**, 420 (1995).
[72] E. Gates, M. Krauss, and M. White, Phys. Rev. D **51**, 2631 (1995).
[73] S. M. Bilenky and C. Giunti, Astropart. Phys. **2**, 353 (1994).
[74] G. Fiorentini *et al.*, Phys. Rev. **49**, 6298 (1994); V. Berezinsky, G. Fiorentini, and M. Lissia, Phys. Lett. B **341**, 38 (1994).
[75] P. I. Krastev and A. Yu. Smirnov, Phys. Lett. B **338**, 282 (1994).
[76] P. I. Krastev, S. T. Petcov, and L. Qiuyu, Phys. Rev. D **54**, 7057 (1996).
[77] P. I. Krastev and S. T. Petcov, Phys. Lett. B **299**, 99 (1993).
[78] The Sudbury Neutrino Observatory Collaboration, Phys. Lett. B **194**, 321 (1987); G. T. Ewan *et al.*, ''Sudbury Neutrino Observatory Proposal,'' Report No. SNO-87-12, 1987 (unpublished); ''Scientific and Technical Description of the Mark II SNO Detector,'' edited by E. W. Beier and D. Sinclair, Report No. SNO-89-15, 1989 (unpublished).
[79] S. Goswami, K. Kar, and A. Raychaudhuri (in preparation).
[80] Y. Z. Qian *et al.*, Phys. Rev. Lett. **71**, 1965 (1993).
[81] K. S. Babu, R. K. Schaefer, and Q. Shafi, Phys. Rev. D **53**, 606 (1996).